Experimental study of flow modification inland from a coast for nonneutral conditions

Sempreviva, Anna Maria; Larsen, Søren Ejling; Mortensen, Niels Gylling

Publication date:
1992

Document Version
Publisher's PDF, also known as Version of record

RISØ

Risø-M-2924(EN)

Experimental Study of Flow Modification Inland from a Coast for Nonneutral Conditions

Anna M. Sempreviva, S.E. Larsen and N.G. Mortensen

Risø National Laboratory, Roskilde, Denmark
January 1992

Experimental Study of Flow Modification Inland from a Coast for Nonneutral Conditions

Risø-M-2924(EN)

Anna M. Sempreviva[1], S.E. Larsen and N.G. Mortensen

[1]On leave from Istituto di Fisica dell'Atmosfera, C.N.R., Rome, Italy

Risø National Laboratory, Roskilde, Denmark
January 1992

Abstract

During a two-year period, measurements were obtained along four meteorological masts placed from the coastline to 30 km inland at the North Sea coast of Jutland in Denmark (the JYLEX experiment).

The data were organized to show the behaviour of the most important parameters of the turbulent structure when a flow passes from over-sea to over-land conditions. The results are stratified according to season, day and night, and wind direction.

ISBN 87-550-1719-3
ISSN 0418-6435

Grafisk Service · Risø · 1992

Contents

1 Introduction

When air flows from one surface to another with different characteristics, an Internal Boundary Layer (IBL) develops downwind from the change. For long fetches the IBL grows until it fills in the Planetary Boundary Layer (PBL), and a new equilibrium is established. In this paper we shall relate the problems of a flow response to changing surface characteristics to a data set obtained during an experiment (JYLEX) in which meteorological parameters were measured along four masts placed inland from the coastline at the North Sea coast of Denmark.

In an earlier paper (Sempreviva et al., 1990) we have discussed the development of an IBL when controlled by mechanical turbulence only, that is near-neutral conditions. Here, we pay attention to the problem of the growth of an IBL over land when thermal effects are important.

The flow response will be discussed in terms of a data set analysis with production of spatial variation of the characteristic parameters of the atmospheric turbulence.

2 Experimental setup

The JYLEX experiment (JYLland EXperiment) was established on the west coast of Jylland (the Danish name for Jutland) to study the change of surface layer characteristics as a function of distance from the sea.

Meteorological variables were measured along four masts placed from the shore line up to 30 km inland. The positions of the masts are shown in Fig. 1. The shore-line mast M1 was a 32-m mast while the rest of the masts were 24 m high. Figure 2 illustrates the appearance of the shore-line mast and one of the inland masts. Table 1 summarizes the measurements conducted at each mast.

The experiment lasted from May 1982 until June 1984 yielding 25 months of data. The measurements were recorded as 10-min average values while wind direction and temperature were recorded as instantaneous values, although the response time of the instruments themselves provided some smoothing. The time constants of the wind vanes were about $20/u$ (u being wind speed measured in m/s) while the thermometers had time constants of around 2 min; both values are from Mahrt and Larsen (1982) who used the same instrumentation.

In connection with change of recorder tapes (every three weeks), photographs were taken of the surroundings of each mast to record seasonal variation of the vegetation.

The experiment was originally conceived as a straight line of masts reaching from the west coast of Jutland towards the east. It appears from Fig. 1 that the final setup neither started at the shore line of the North Sea nor can it be described as a straigth line. To avoid flow-obstructing features in the near field around each mast had the highest priority, and the final setup was a result of this. Even in this fairly flat part of Denmark, such features were abundant in the form of coastal brinks, dues, and dikes at the coast or hills, houses and trees further inland.

A more detailed description of the measuring site with roughness, distance to the coast etc. is given in Sempreviva et al. (1988).

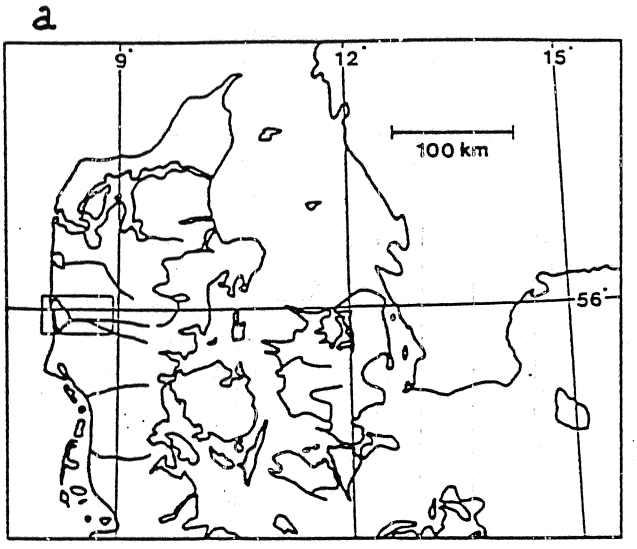

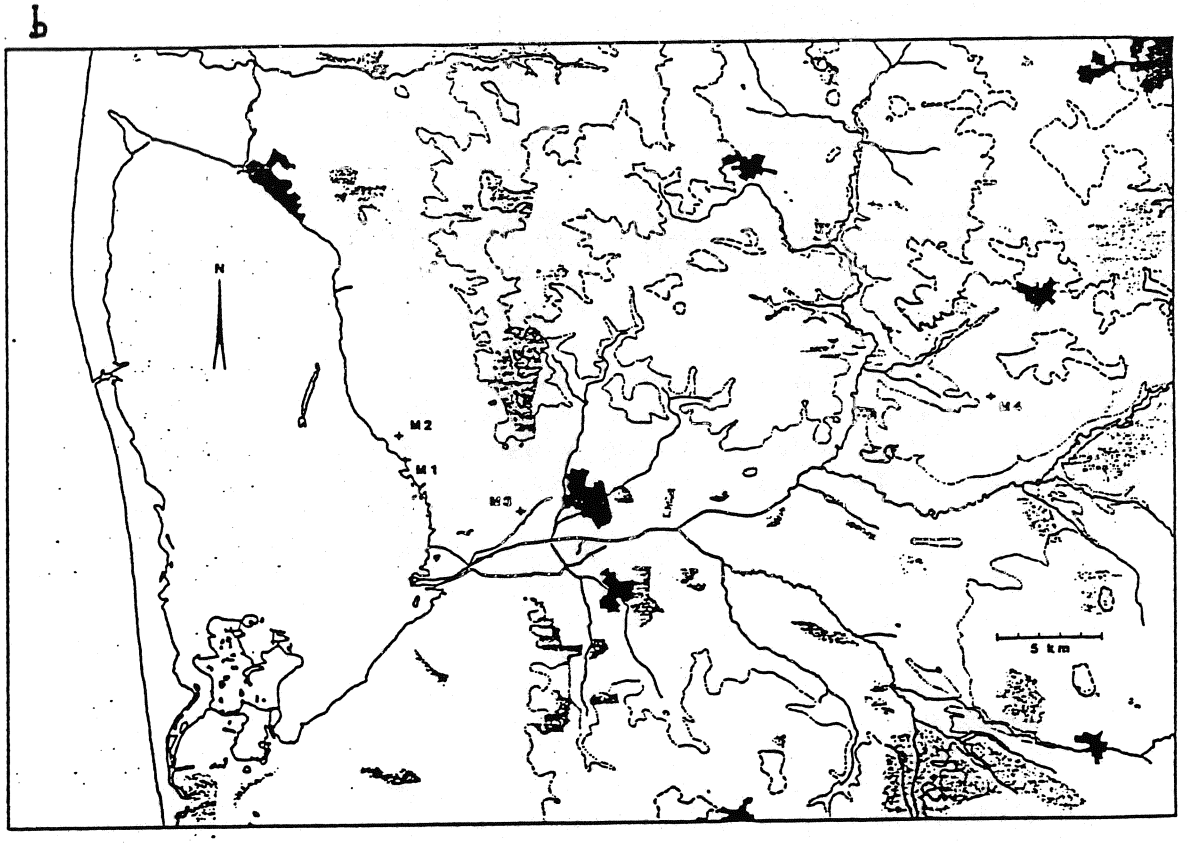

Figure 1. Maps of the experimental site. Figure 1a shows the overall area while Fig. 1b gives a more detailed map of the site, indicating positions of the masts. In Fig. 1b main geographical features are also indicated, such as towns (black areas), forests (shaded areas), and heights of terrain (20 and 50-m isolines). Positions of the measuring masts are indicated by M1, M2, M3, and M4).

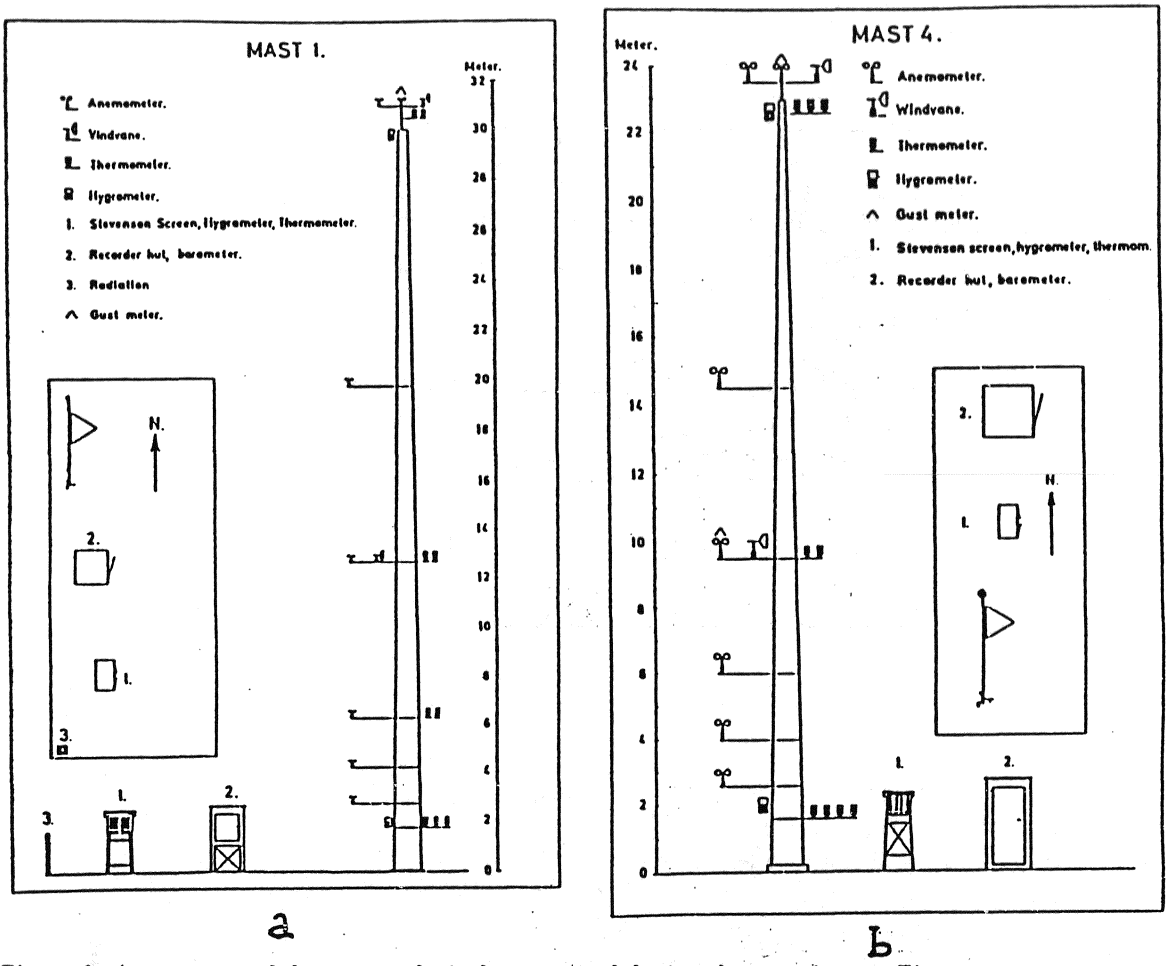

Figure 2. Appearance of the meteorological masts used during the experiment. Figure 2a shows the mast at the shoreline, mast 1, while Fig. 2b shows one of the inland masts, mast 4.

3 Data selection and analysis

The present paper is concerned with the change of turbulence characteristics as the air moves from the sea under nonneutral conditions, considered in a previous paper (Sempreviva et al., 1990). Therefore, a subset of data was selected according to the following criteria:

- data were to be included only in case of wind from the westerly sectors at mast 1, that is between 235 and 315°;
- data should be available at all four masts, and
- data with nonneutral conditions were ensured by demanding that the calculated Richardson number Ri should fulfill the following conditions at all four masts

$$Ri < -.03 \qquad Ri > .03$$

The selected data set consisted of 18025 profiles simultaneously recorded at each mast, specified below according to season and wind direction sector.

Table 1. Distribution of the nonneutral data used in this report according to wind direction sectors (1–9, see below) and season.

Wind Dir. Sector	1	2	3	4	5	6	7	8	9	Total
Winter	747	845	926	938	755	756	799	544	387	6697
Spring	154	118	123	120	134	132	126	226	257	1390
Summer	434	476	575	598	725	775	928	1265	1855	7631
Fall	123	231	386	238	207	166	210	350	396	2307
Total	1458	1670	2010	1894	1821	1829	2063	2385	2895	18025

The smaller number of cases for spring and fall is due to the definition of periods, i.e. the periods of spring and fall are shorter than those of winter and summer, defined the normal way. Each set was stratified and codified according to the following criteria.

Wind direction sectors

The 90° sector was subdivided into nine 10° sectors. This division into sectors has been done for two reasons.

1. The individual mast looks across different upstream surface characteristics in each sector.
2. At the coastline the upwind air flow has different meteorological characteristic parameters (e.g. humidity, speed, temperature). A flow from the north is generally colder and less moist than one from the south because the former is often associated with high-pressure systems from the polar circle.

Seasons

We did not consider the conventional period for the seasons. We have chosen spring and fall periods in such a way that

a) the same amount of solar radiation would arrive at the ground surface if clouds etc. could be neglected;

b) the periods are supposed to cover as much as possible the periods when $T_{sea} \ll T_{land}$ and $T_{sea} \gg T_{land}$ for spring and fall, respectively. As a result we use seasons defined as follows.

winter	30.10	–	09.03
spring	10.03	–	12.05
summer	13.05	–	31.07
fall	01.08	–	29.10

In Fig. 3 the yearly behaviour of the air and sea temperature is shown (Larsen and Jensen, 1983). In the cited report the authors found that climatologically seen the sea temperature in the spring is 1° colder than the air temperature.

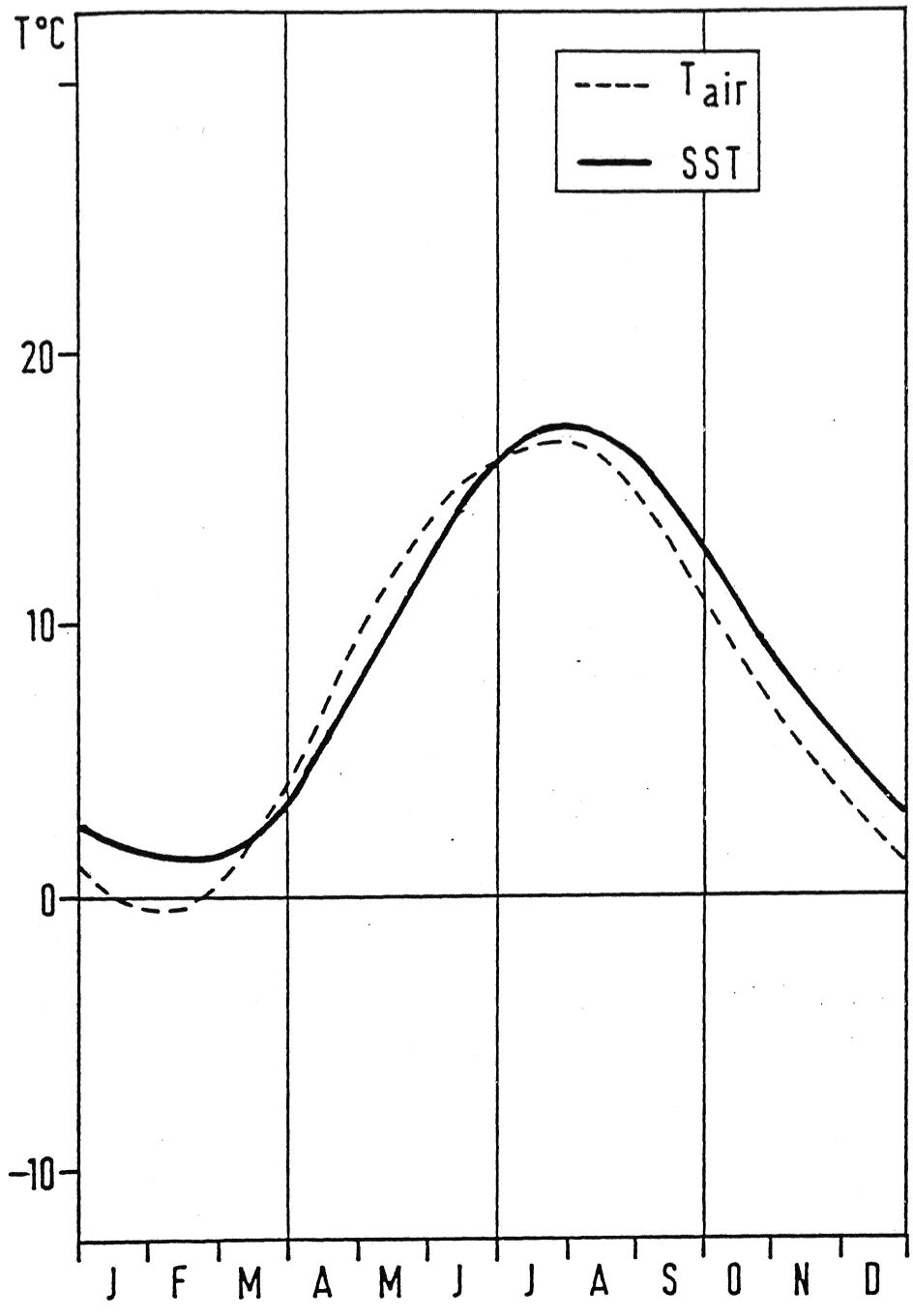

Figure 3. The annual variation of Danish national average values of air and sea surface temperature (Larsen and Jensen, 1983).

Day and night

The time of sunset and sunrise has been calculated for each day of the year by simple library routines and compared with the values from standard tables. For each 10-min scan the following parameters have been calculated.

Richardson number

$$Ri = \frac{g}{T} \frac{\frac{\delta T}{\delta z} + \Gamma}{\left(\frac{\delta \bar{u}}{\delta z}\right)^2} \tag{1}$$

where the detailed definitions are specified in Appendix A. The reference height used for the Richardson number calculation was 10 m.

Monin-Obukhov length L

This was calculated using the Richardson number. To avoid that for $Ri > 0.2$ L goes to infinity and then turns to positive values, we used the formulation given in Appendix A, Eqs. (A9) and (A10) (Larsen and Nielsen, 1991)

$$L = \frac{T}{g\kappa} \frac{u_*^2}{T_*} \tag{2}$$

Depending on the sectors, mast 1 is located at a distance varying betweeen 75 and 1100 from the coast. For each direction we plotted the wind profiles, see figure 4.

From the plots a kink is seen showing two profiles, a lower and an upper one. The kink disappears with increasing distance to the water because of homogeneous terrain from the mast (figure 4, sectors 8 and 9). It is also seen that the sector profiles can be divided into groups according to the upwind flow climatology.

From these profiles we may guess that data from the higher levels of the mast, viz. 13 and 30.9 m, for temperature and 19 and 31.5 m, respectively for wind speed represent over-water conditions while the lower levels measure the parameters pertaining to the IBL that develops when air flows inland from the sea. With this in mind we calculated as follows.

Temperature over sea at 2 m

We used the upper-level temperature to calculate the temperature over the sea at 2 m, using similarity profiles of potential temperature, compare Appendix A.

In table 2 the values of the two temperatures are shown for each season and day and night. The two temperatures should represent two different situations. The extrapolated temperature should represent over-sea conditions and the measured temperature the IBL conditions.

As could be expected from figure 4 for sector 9 (with the longest fetch, i.e. 1150 m to the water), the two temperatures have the same values showing an homogeneous upwind terrain. The sector also shows the larger difference between day and night temperature which also indicates that in this sector mast 1 mostly reflects land conditions.

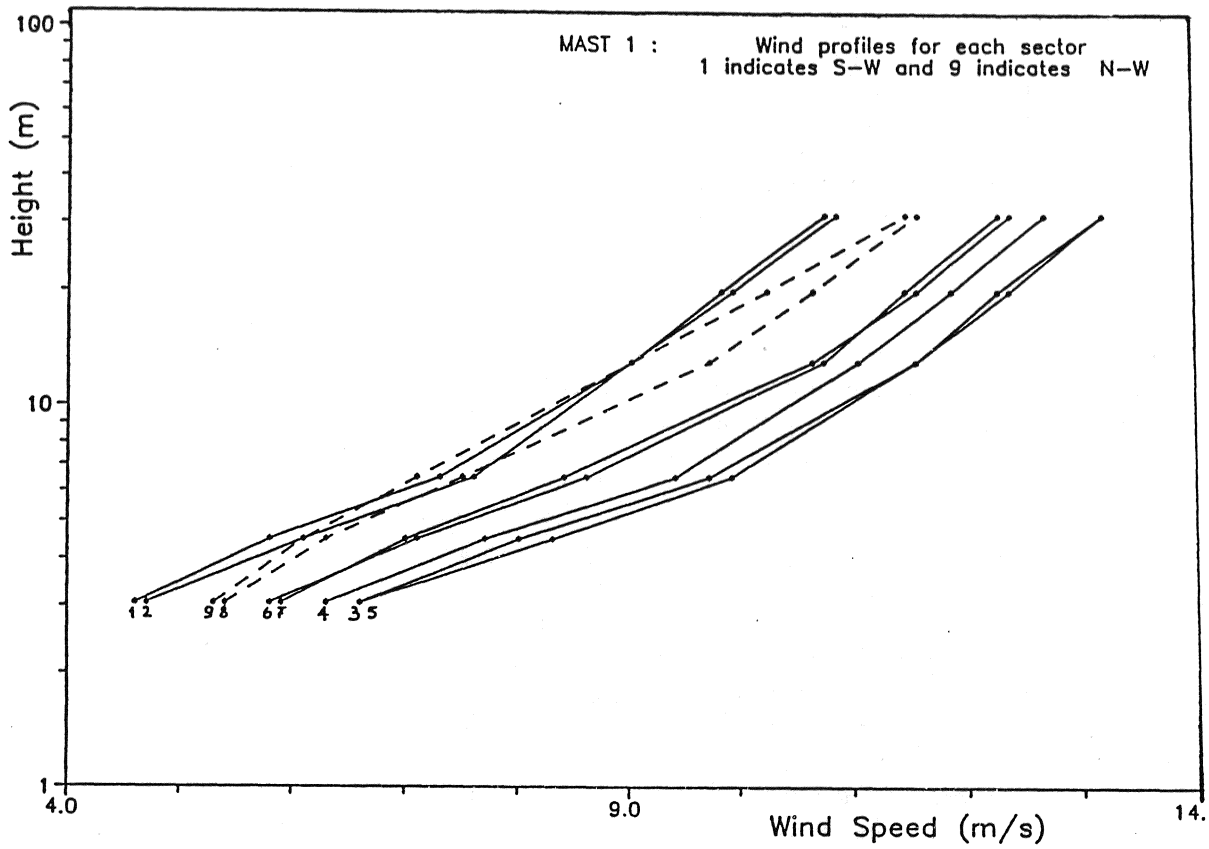

Figure 4. Mast 1: wind profile averages over the data summarized individually for each wind direction sector in table 1.

Table 2. Variability of temperatures at mast 1 versus season, time of day and sector. T_{land} is the temperature measured 2 meters above local terrain. On the other hand, T_{sea} is the temperature at 2 m extrapolated from the measurements at 13 and 31 m, respectively. These temperatures are assumed to mostly reflect upstream over-sea conditons.

Sector	Winter				Spring				Summer				Fall			
	Day		Night		Day		Night		Day		Night		Day		Night	
	T_{land}	T_{sea}	T_{land}	T_{sea}	T_{land}	T_{sea}	T_{land}	T_{sea}	T_{land}	T_{sea}	T_{land}	T_{sea}	T_{land}	T_{sea}	T_{land}	T_{sea}
1	6.9	6.6	7.0	6.8	7.1	6.6	5.5	5.7	14.3	14.1	14.4	14.8	17.0	16.7	16.2	16.4
2	7.7	7.3	6.7	6.5	5.7	5.5	5.2	5.5	14.3	14.1	12.9	13.2	16.4	16.3	16.4	16.6
3	8.7	8.5	6.5	6.3	5.5	5.3	5.1	5.2	14.0	13.9	12.7	13.0	16.7	16.4	16.6	16.8
4	7.7	7.6	7.3	7.3	5.4	5.3	5.2	5.4	14.0	13.8	12.9	13.2	16.5	16.1	15.3	15.4
5	6.8	6.7	6.6	6.6	6.1	5.8	4.9	5.1	13.9	13.9	13.0	13.3	15.7	15.2	14.5	14.5
6	7.0	6.8	6.4	6.4	6.6	6.3	4.4	4.7	14.2	14.1	12.4	12.8	15.8	15.7	14.2	14.2
7	7.3	7.0	6.3	6.3	7.1	7.0	4.8	4.9	14.1	14.1	12.7	13.0	16.0	16.0	13.5	13.9
8	7.9	7.8	5.9	5.9	8.1	7.9	5.8	6.0	13.8	13.8	12.3	12.5	15.8	15.8	12.8	13.0
9	8.3	8.2	5.6	5.5	8.1	8.1	5.9	6.1	13.8	13.9	12.0	12.1	16.3	16.2	13.4	13.4

Wind speed ratios U_i/U_1

The ratios between the values of the velocity at mast i = 2, 3, and 4, and the value at mast 1 have been calculated (where the velocities refer to 24 m.) At mast 2, 3, and 4 the measurement level is 24 m while for mast 1 we extrapolated the 31.5 m velocity to 24 m using upstream parameters.

Sensible heat flux

$$\text{heat flux} = -\rho\, c_p T_* u_* \tag{3}$$

where ρ is the air density, c_p the specific heat at constant pressure, T_* the turbulence temperature scale, and u_* is the friction velocity.

For mast 1 heat flux was calculated using the 13 and 31 m level, respectively, while for the other masts the 2 and 24-m levels were used.

To test the applied methods (see Appendix A), we considered mast 3 where also a sonic anemometer was used. A complete 24-hour time series of heat fluxes was selected for 28 June 1983, computed by eddy correlation and compared with correlations calculated in Eq. (3). Figure 5 shows this comparison. As it can be seen, the two time series show good agreement.

Finally, a few words should be said about the analysis approach in the present report. The purpose is mostly to extract the broad climatological features of the JYLEX data set of most relevance to the growth of the internal boundary layer when thermal effects are important. Therefore, our approach shall be to average the parameters above specified for each of the classes also defined above, that is for each mast, wind direction sector, season and day/night.

It is to be noted that a set of stability classes has not been defined as would have been natural in this study of nonneutral boundary layers. The reason is our difficulty in specifying relevant stability classes here where both the stability over water and over land are relevant. Furthermore, it is not clear at present that stability would be the best measure of the influence of thermal effects on the growth of the internal boundary layer. As a rough measure of the thermal effects, the seasons and day/night stratification are used here.

As in the study of neutral JYLEX data (Sempreviva et al., 1989), we use the wind direction stratification to plot the data versus land fetch although realizing that this method is more doubtful in the present report as the insolation characteristics are found to be different for different wind directions.

4 Presentation of the figures

In this section we present a series of figures that illustrates the climatology of the region for characteristic parameters important to the formulation of models that describe development of a thermal internal boundary layer TIBL.

In Fig. 6a the incoming global solar radiation pertaining to each wind direction is shown. Unfortunately, only one year of data was available for this parameter, but the comparison between analyses for the said year and/or for the complete set of data shows largely the same results as exemplified in Fig. 6b.

We obtained a set of 10266 10-min data points with radiation measurements. Their distributions according to sectors and season are shown in table 3.

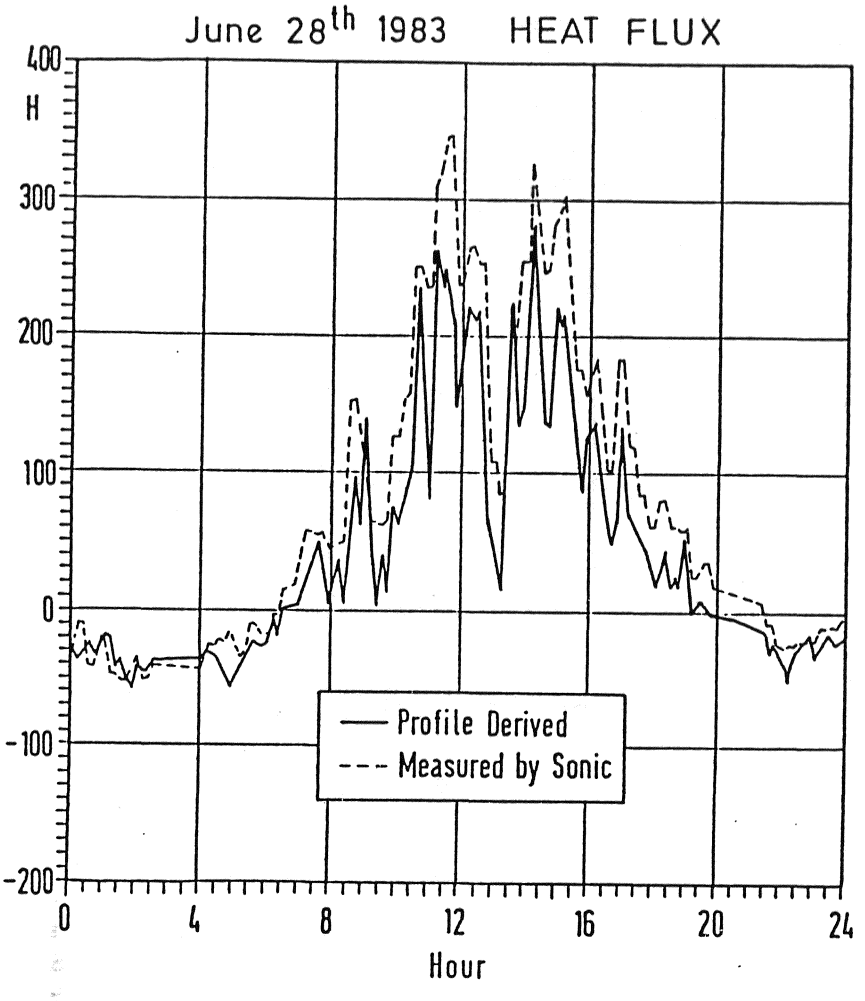

Figure 5. Comparison between the heat flux estimated by a sonic anemometer and the velocity and temperature profiles as used in this report and detailed in Appendix A.

Table 3. Distribution of the radiation data according to wind direction sectors (1 - 9) and season.

Season	1	2	3	4	5	6	7	8	9	Total
Winter	227	349	494	369	209	245	285	178	179	2535
Spring	49	39	18	3	24	31	26	91	142	423
Summer	281	340	418	396	411	465	642	953	1409	5315
Fall	116	213	267	216	199	148	181	301	352	1993
Total	673	941	1197	984	843	889	1134	1523	2082	10266

The small number of cases for spring and fall has been discussed before in connection with table 1. For table 3 the spring data are especially sparse due to missing data for that period.

Figures 7 to 12 show the spatial variation of wind speed ratios, friction velocity, scale temperature, Richardson number, vertical and horizontal temperature and heat fluxes resulting from the data analysis.

In the figures presenting the data we shall generally adhere to the notation given in table 4 to distinguish between data from different wind direction sectors.

Table 4. Notation used to distinguish between data from different direction sectors. In most of the plots the data are presented sector by sector. However, we have occasionally grouped the data in three times three neighbouring sectors.

Sector		Sectors	
1	×	1 2 3	*
2	+	4 5 6	■
3	□	7 8 9	○
4	○		
5	⊠		
6	⊗		
7	■		
8	•		
9	*		

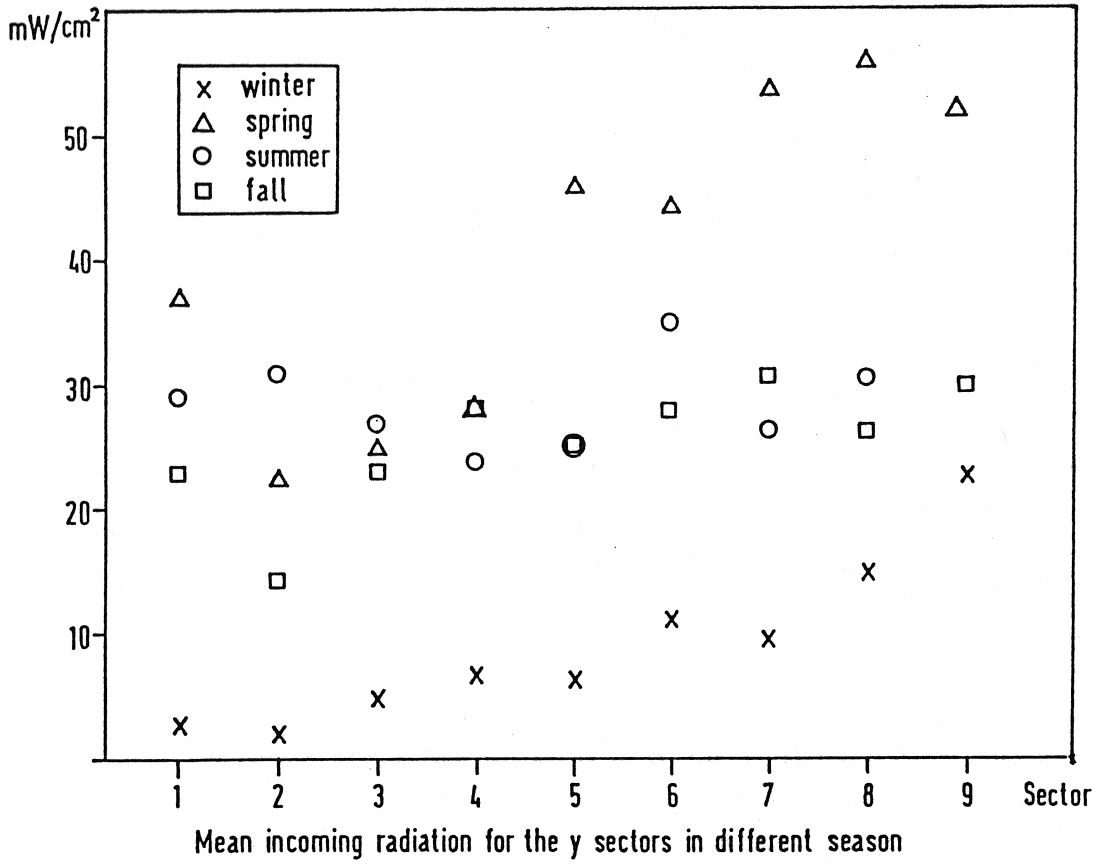

Figure 6a. Global radiation measured at mast 1 as a function of season and wind direction sector.

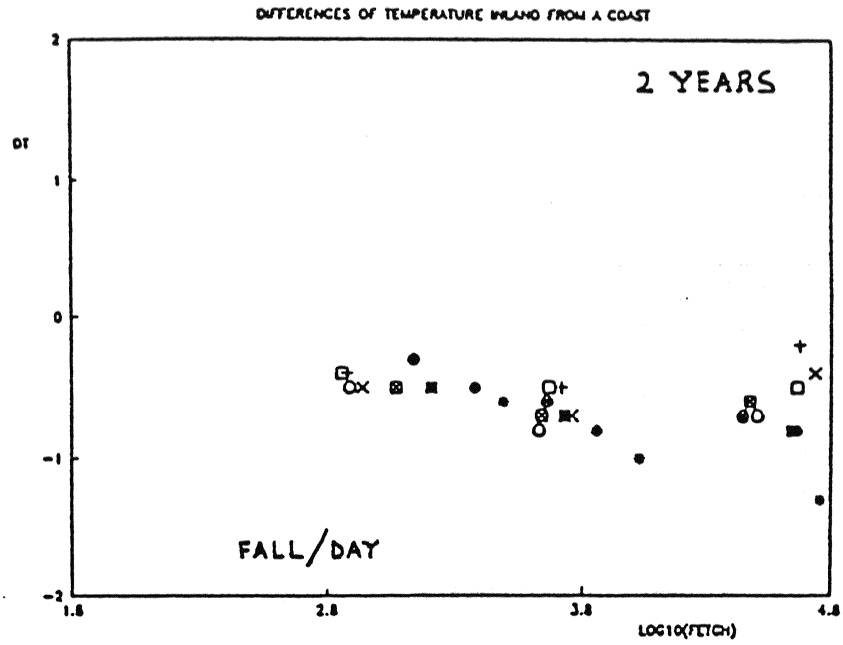

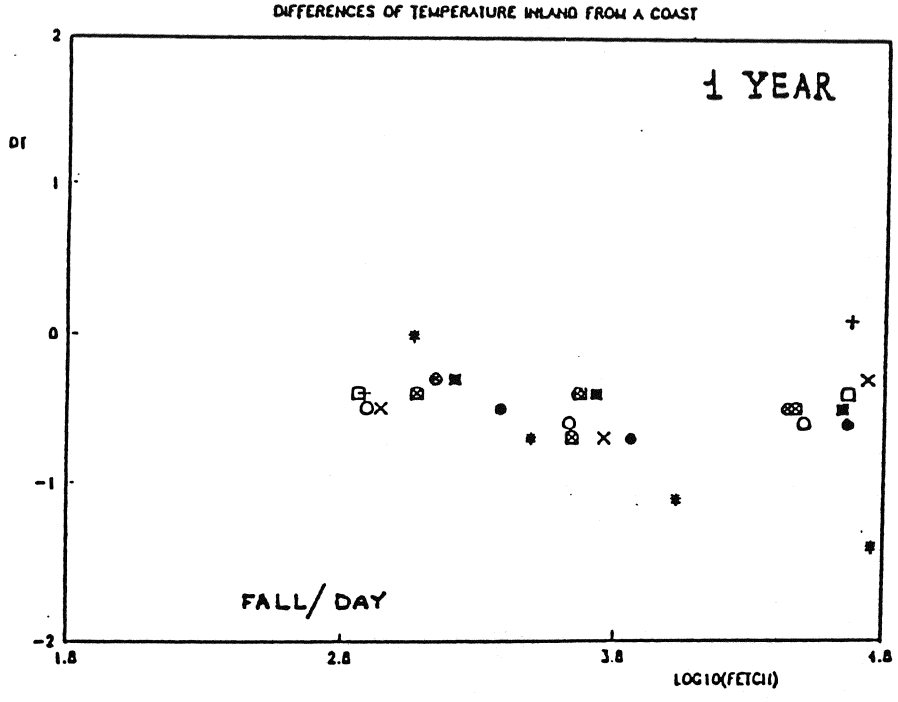

Figure 6b. Difference between the 2-m temperature at mast 2, 3 and 4 and mast 1 for different periods and for the full data set as well as for the one-year data set where radiation data are available. The notation is described in table 4.

5 General Remarks

As we can expect the atmosphere appears to be more stable at night than by day. In winter the spatial behaviour of the parameters shows less diurnal variation. Global incoming solar radiation (Fig. 6) is seen to depend on the wind direction, which is higher in case of northerly wind. This behaviour is present in all seasons and is due to the different climatology of the flow coming from different sectors.

It is therefore natural that also for the parameters, data pertaining to the NW sectors can be distinguished from data with parameters pertaining to SW sectors that show a different climatology of the two air flows.

5.1 Wind speed ratios u_i/u_1

There is a decrease in the wind going inland. This is more enhanced at night: we assume this to be due to the more stable nighttime conditions over land. In some papers, Ogawa and Ohara (1985), Doran and Gryning (1987), Bergström et al. (1988), Van Wijk et al. (1989), wind speeds are reported to be higher over land than over sea. This happens in spite of the larger roughness over land, when stable stratification over sea and unstable stratification over land occur, especially during spring (Bergström et al., 1988).

It appears from the present data set, figures 7a and 7b, that the spring average wind speed ratio shows the following behaviour. The wind speed decreases at mast 2 sited around 1000 m from the coast and increases again at mast 3 at 3000 m. Another decrease takes place at mast 4 (30–60 km inland). This effect can be observed also during winter, but less clear and only from the southern sectors. Generally, it is seen that the mean ratio is less than one.

To study more thoroughly the argument, we investigated the raw data, searching for data that showed stability over sea as calculated at mast 1 and instability over land as calculated at the remaining three masts. We plotted wind speed ratios versus fetches for the three groups of data as shown in figures 7c, 7d and 7e. From these figures we see that first the ratios tend to decrease with increasing fetch whereafter a considerable spreading of the points appears further downstream. This behaviour can be explained by the fact that the flow response is first dominated by change in roughness with stability effects being more important inland.

We note that there are no cases with stability over sea and instability over land both in winter and in the night-time.

5.2 Richardson number

Winter days and nights show the same behaviour, i.e. decreasing stability conditions over land, see figures 8a and 8b. By night the inland mast measures stable conditions in all four seasons. The behaviour of mast 1 is different, showing over-water conditions. In the spring and summer we observe instability whereas stability is observed during fall. We think that this can be due to advection of colder air from the deeper sea while in the fall the advection is heated over shallow water in front of the mast by the radiation during the day. In the fall stable conditions should instead be due to advection of warmer air from the deeper water over shallow water that emits the heat more rapidly.

During the day, solar radiation heats the shallow water creating instability for all three seasons.

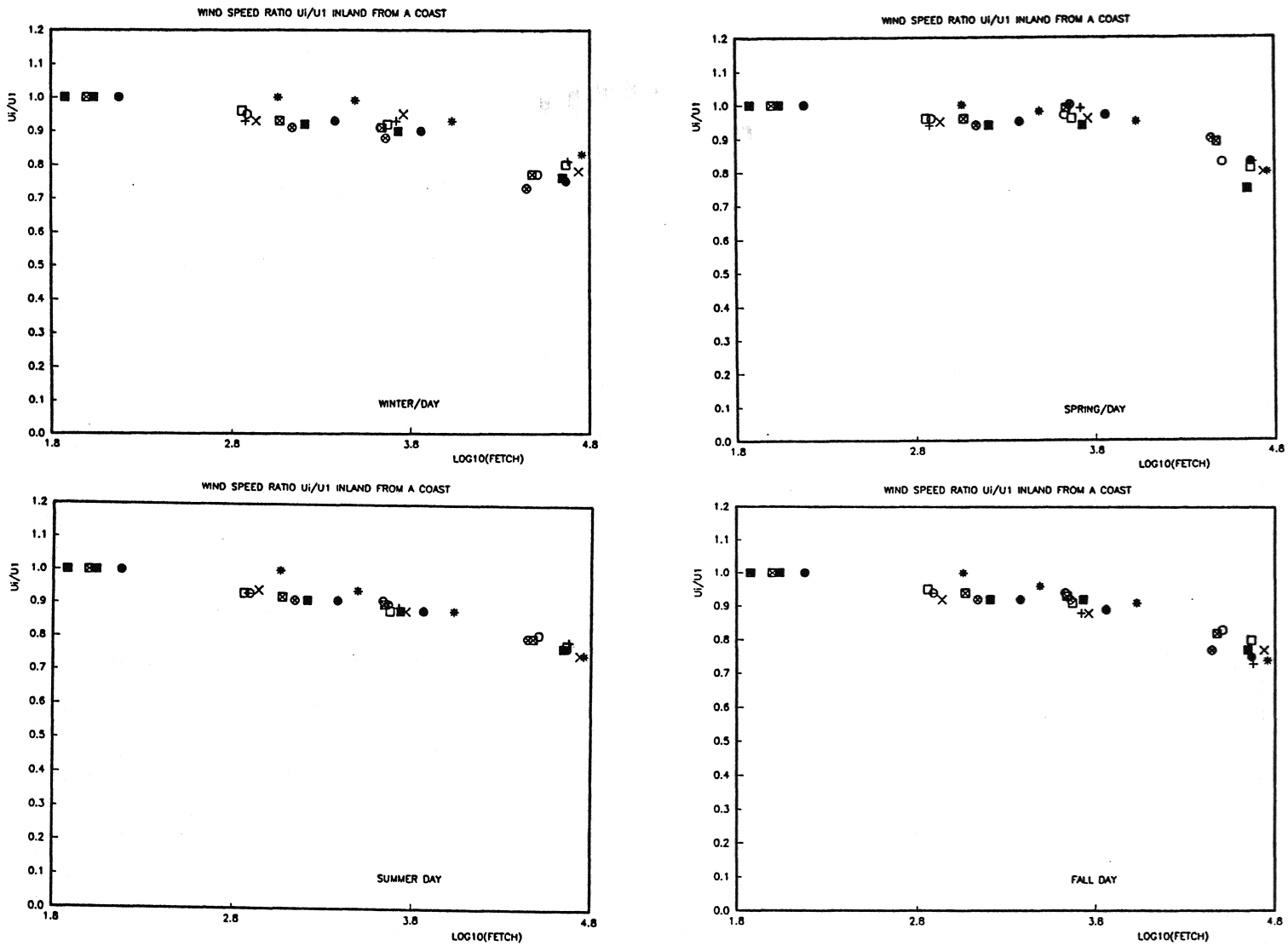

Figure 7a. Ratio between wind speeds at masts i and mast 1 at 24 m. The points are plotted as a function of logarithmic distance [m] to the coast for the different wind direction sectors (different symbols) and masts. Each sector has a specific data symbol, compare table 4.

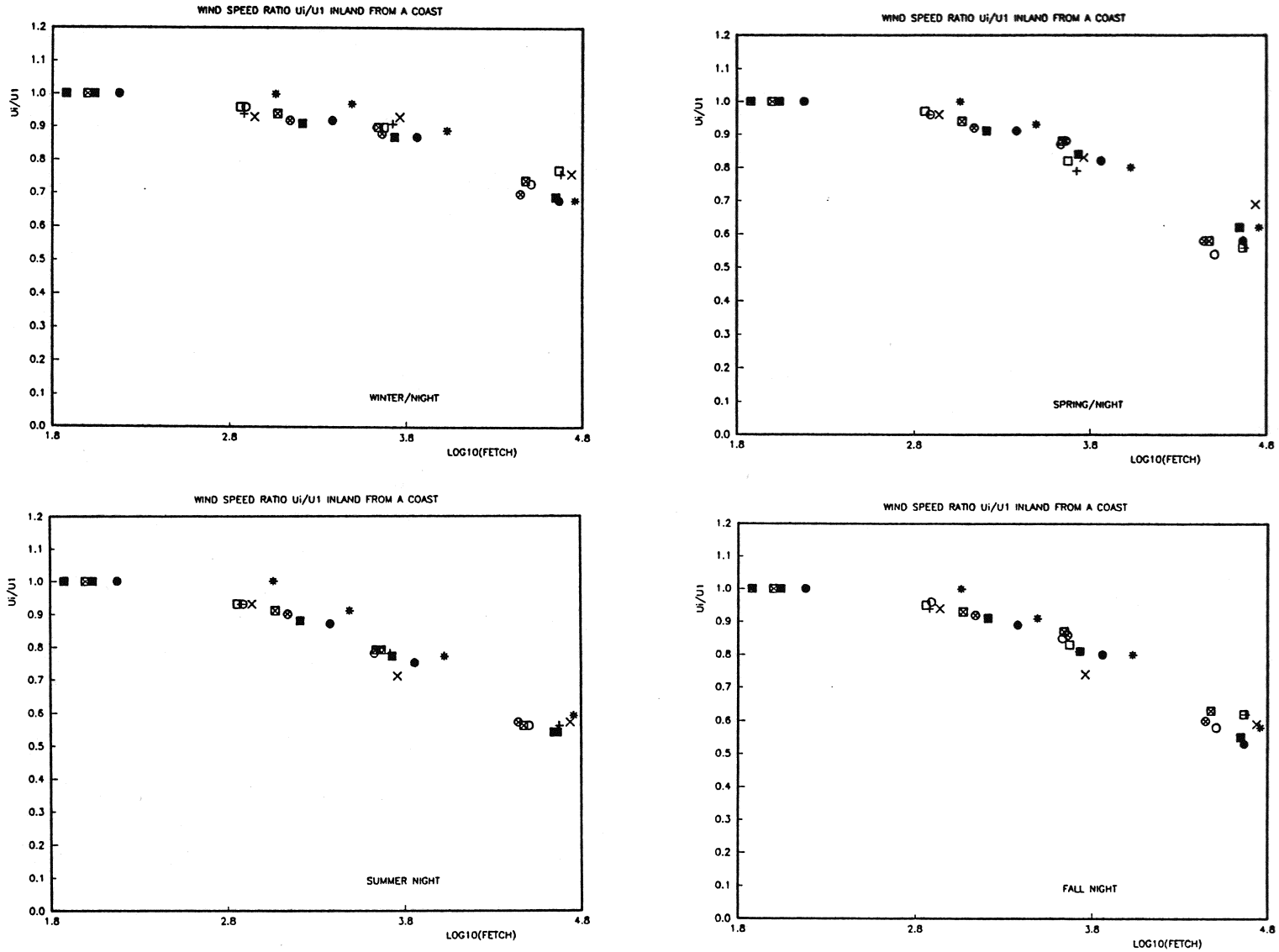

Figure 7b. Ratio of wind speeds for different masts versus logarithm of distance to the coast [m]. See text of figure 7a.

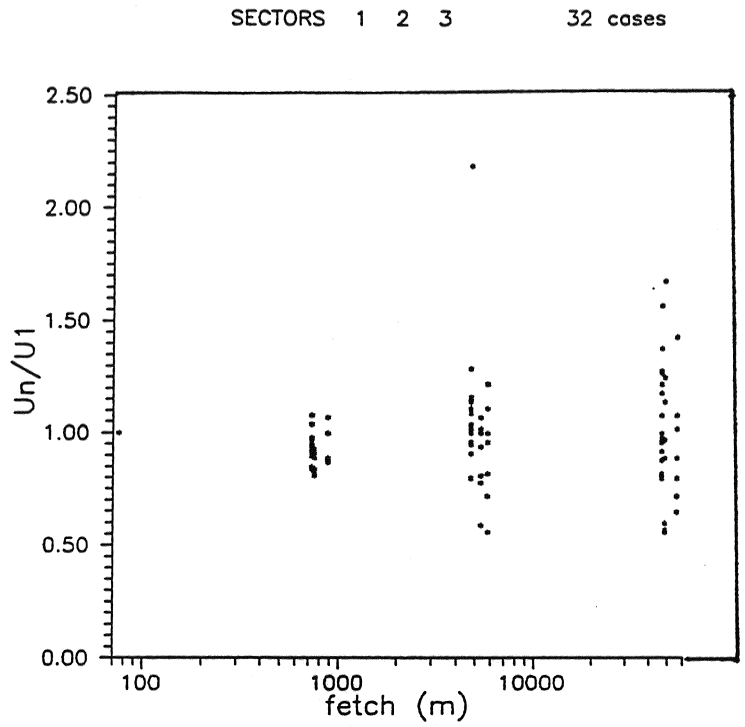

Figure 7c. Wind speed rations plotted versus fetch for selected conditions (stable upstream, unstable downstream at all three land masts) for sectors 1, 2 and 3.

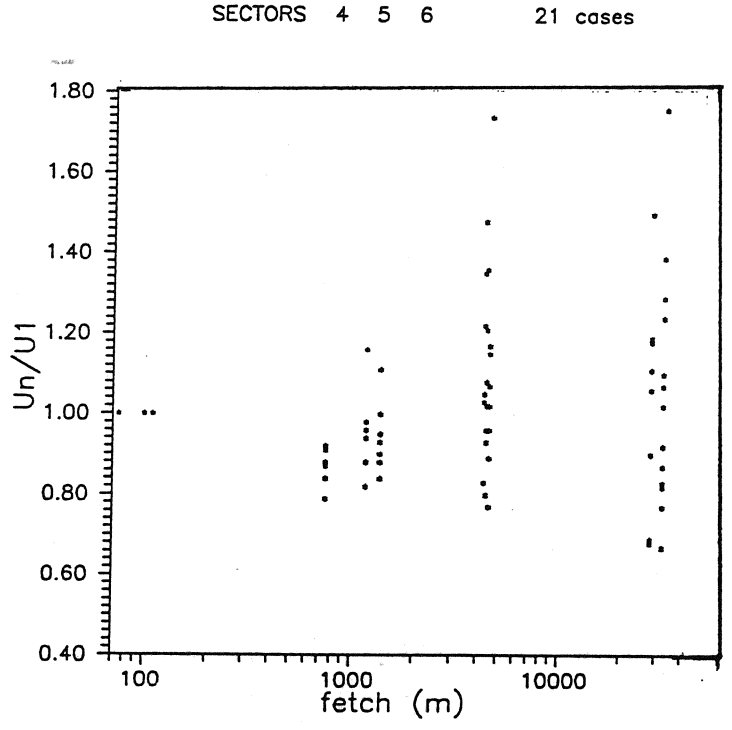

Figure 7d. As for figure 7c but for sectors 4, 5 and 6.

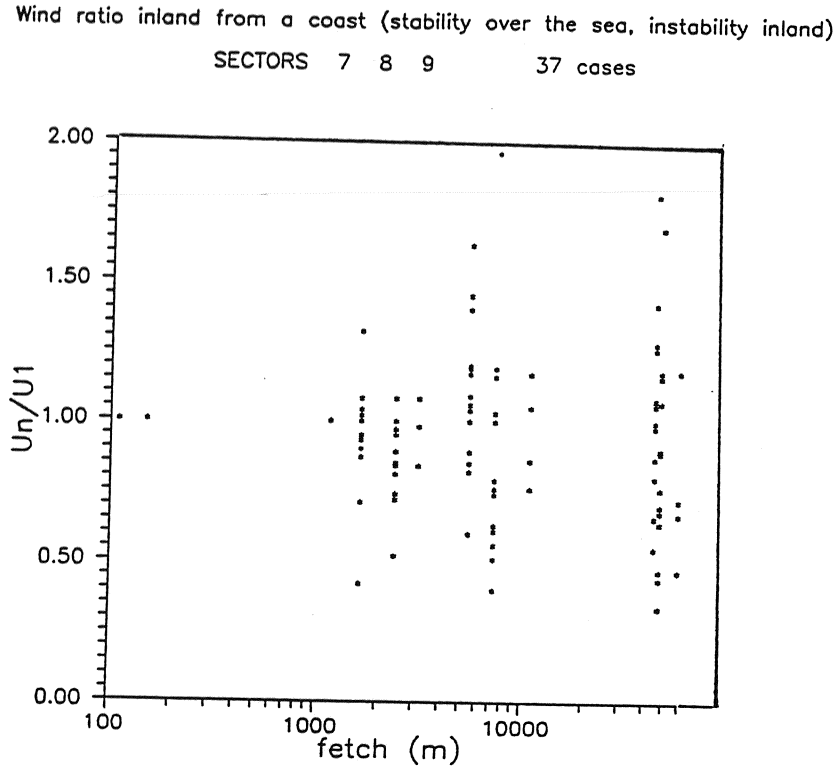

Figure 7e. As for figure 7c and 7d but for sectors 7, 8 and 9.

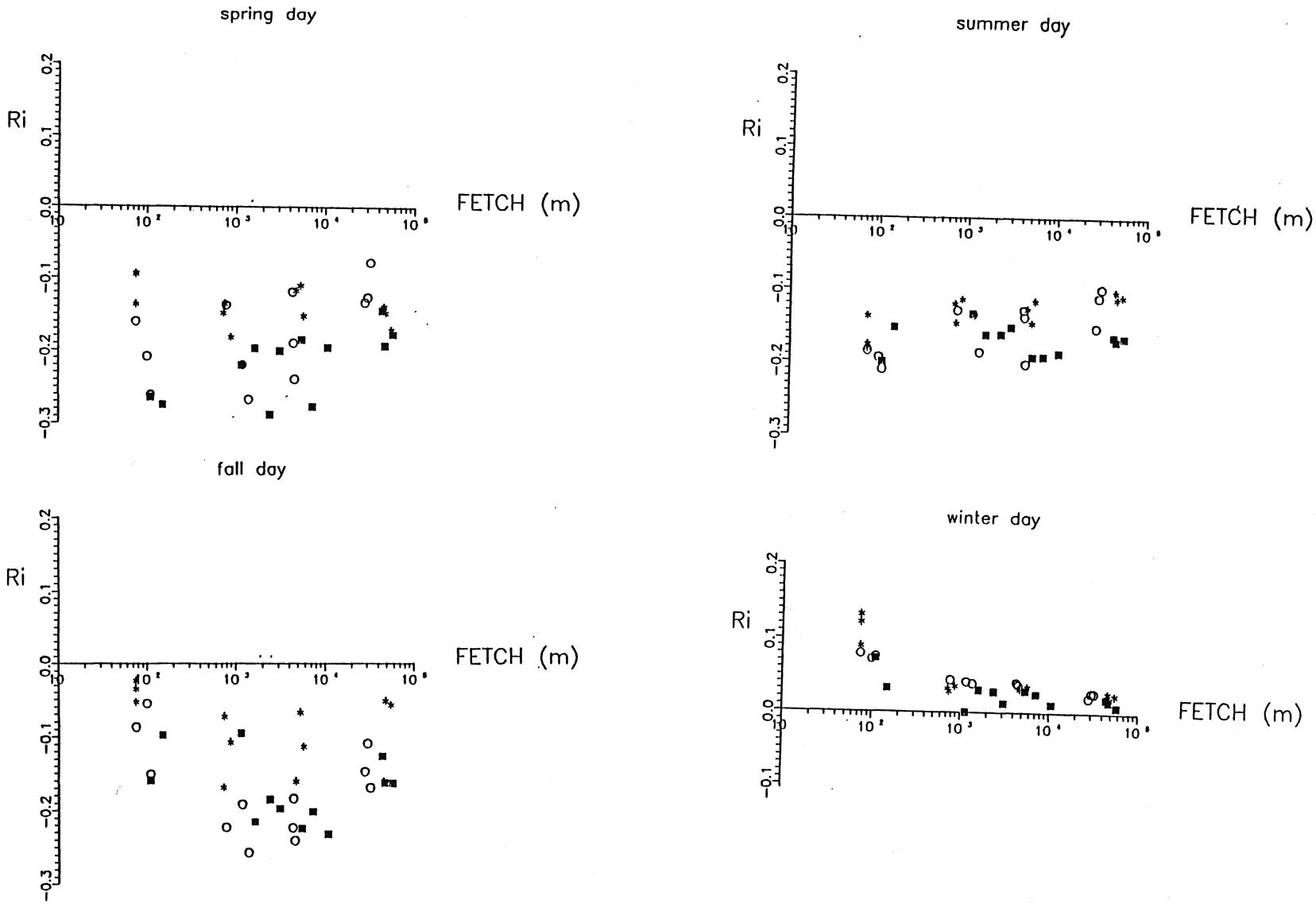

Figure 8a. Richardson number referred to the 10-m height computed for each mast and presented versus fetch, season and day/night. The sector symbols (three by three sectors) are described in table 4.

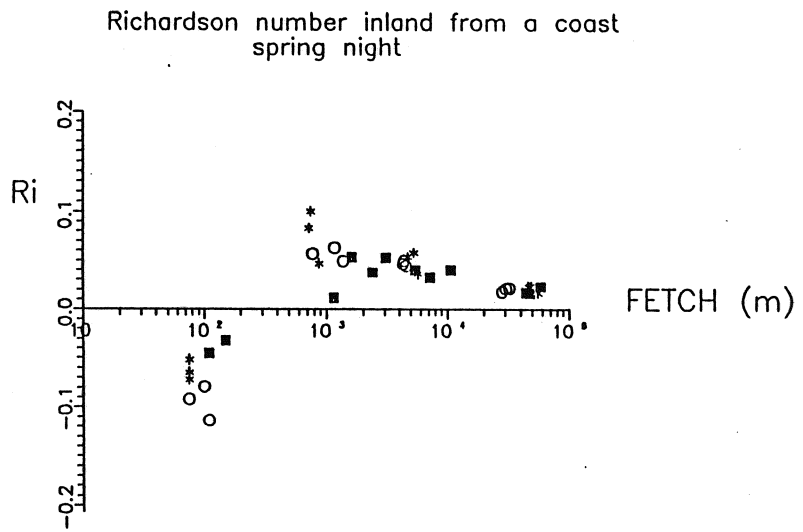

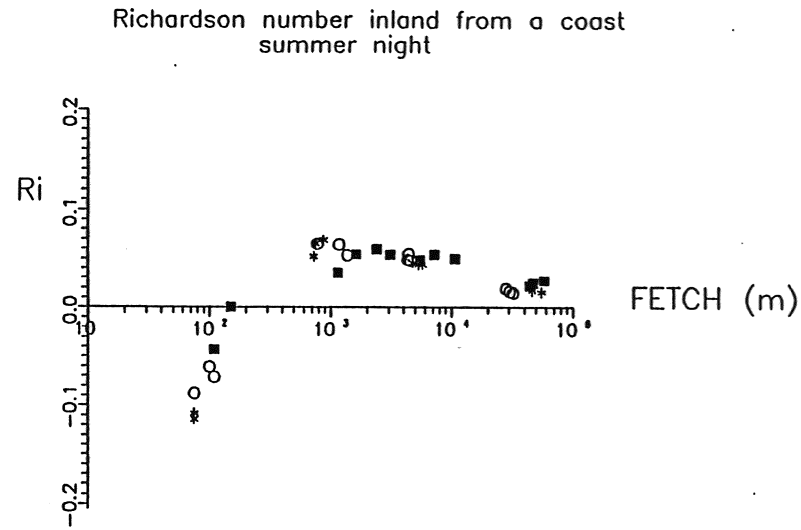

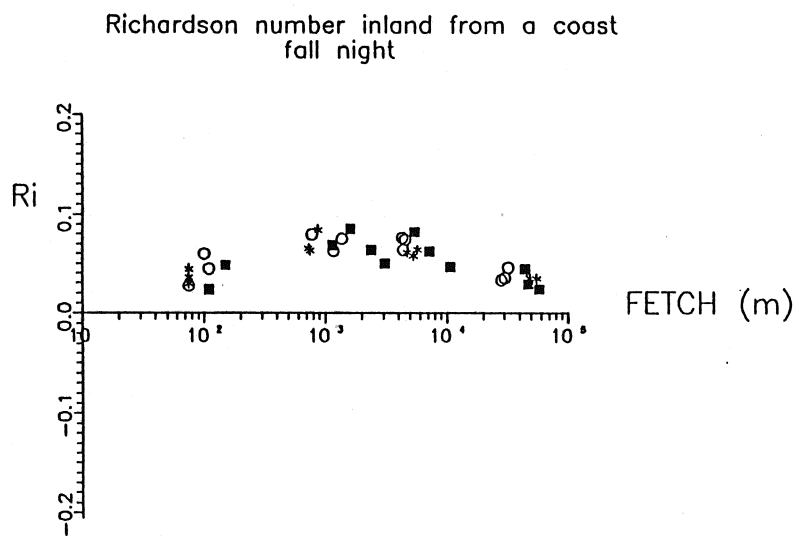

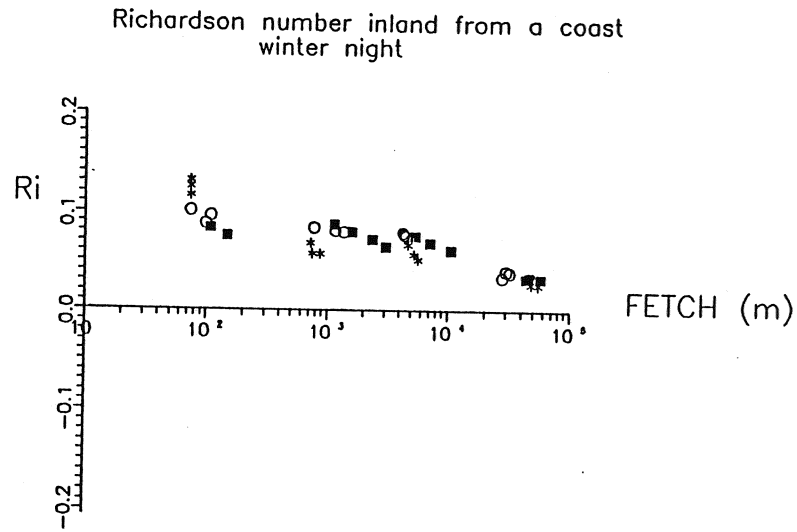

Figure 8b. As for figure 8a.

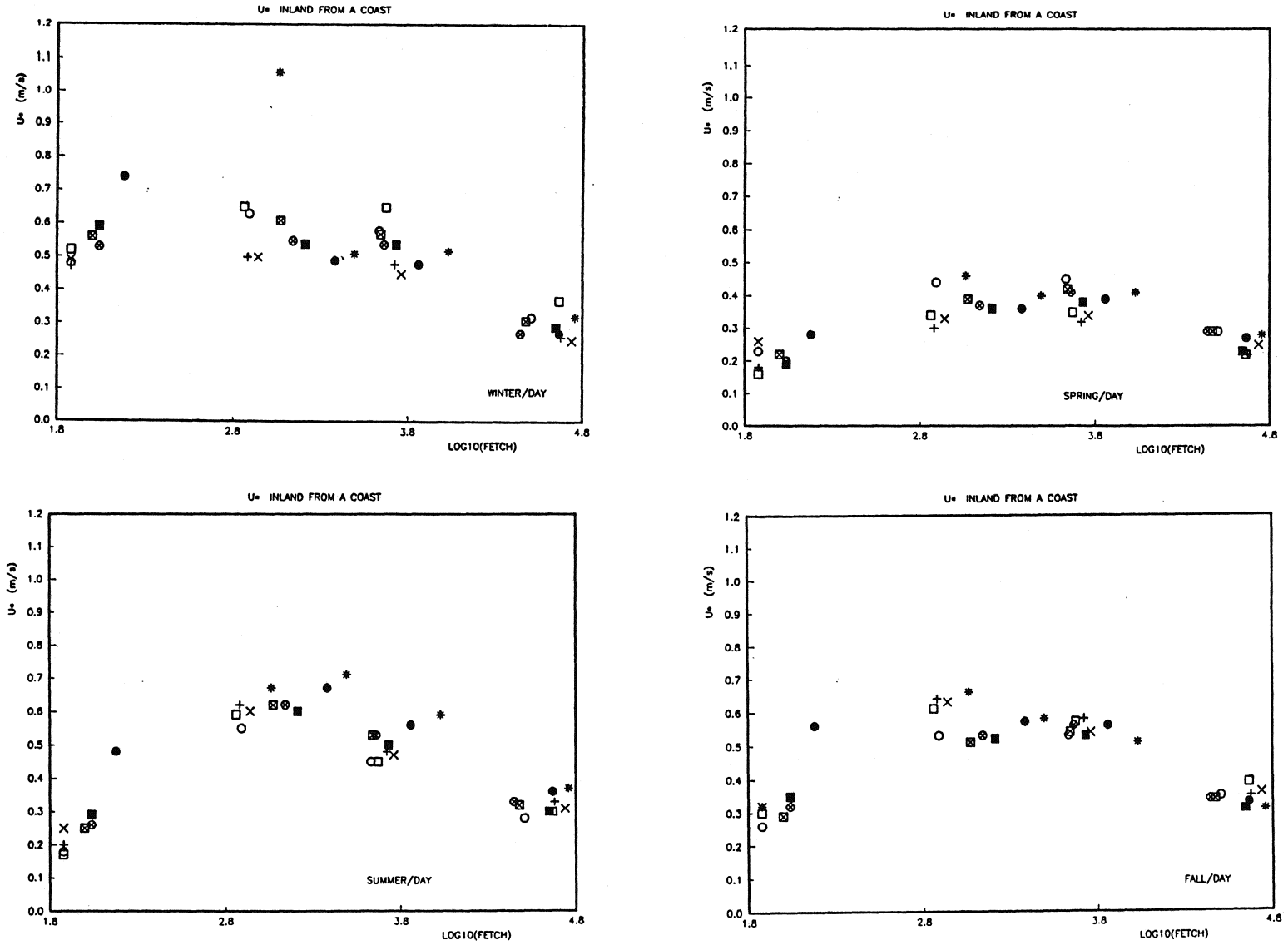

Figure 9a. The u_*-values averaged for each mast, sector, season, day/night and shown versus fetch [m]. The symbols used are explained in table 4.

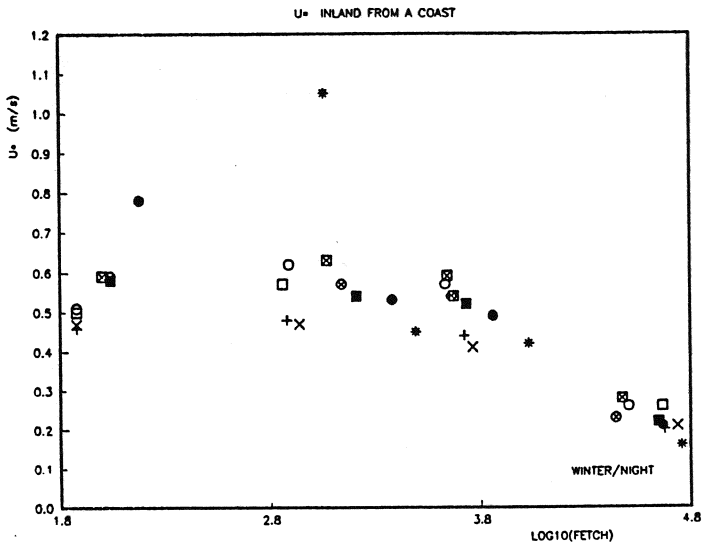

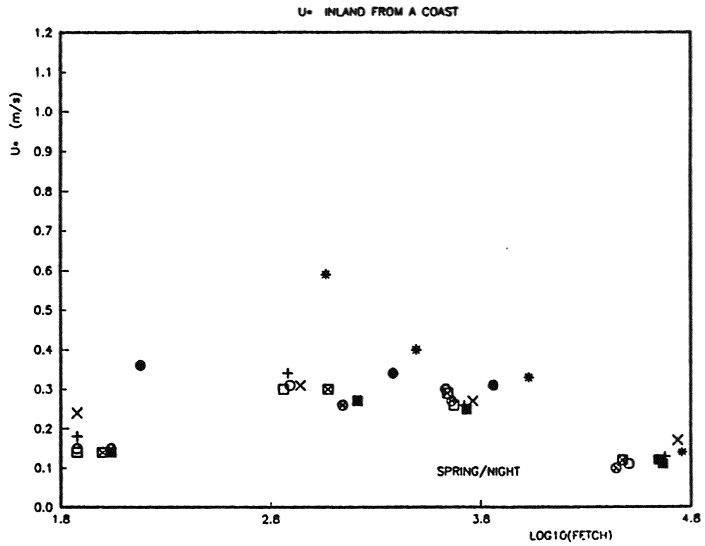

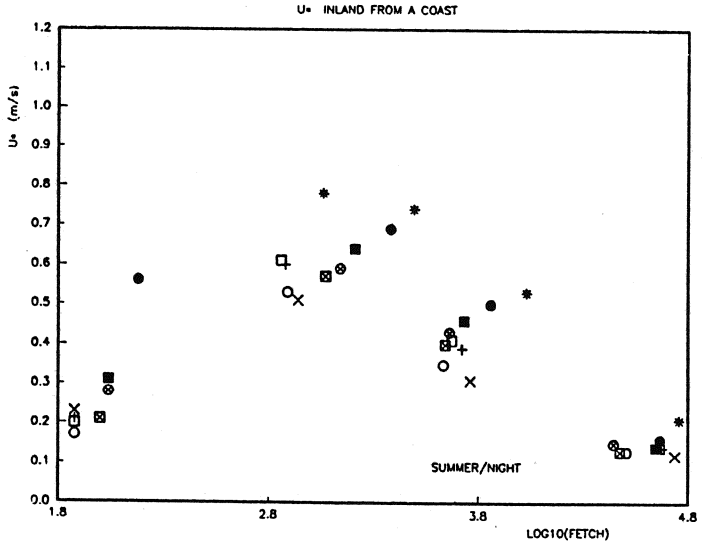

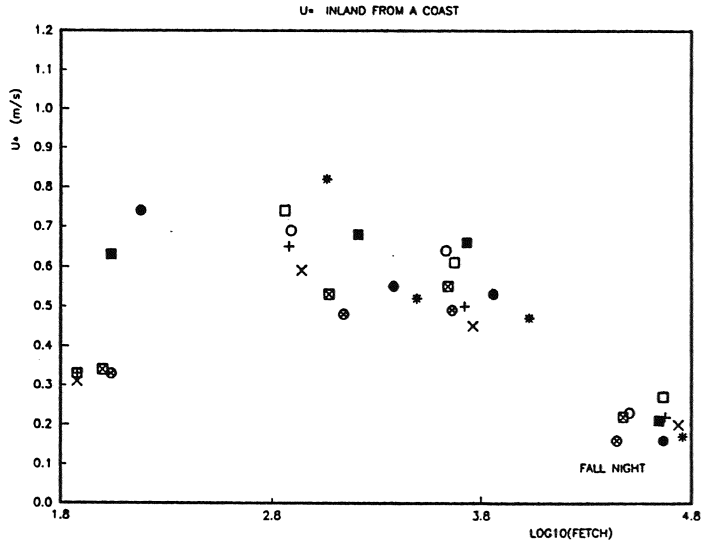

Figure 9b. As in figure 9a.

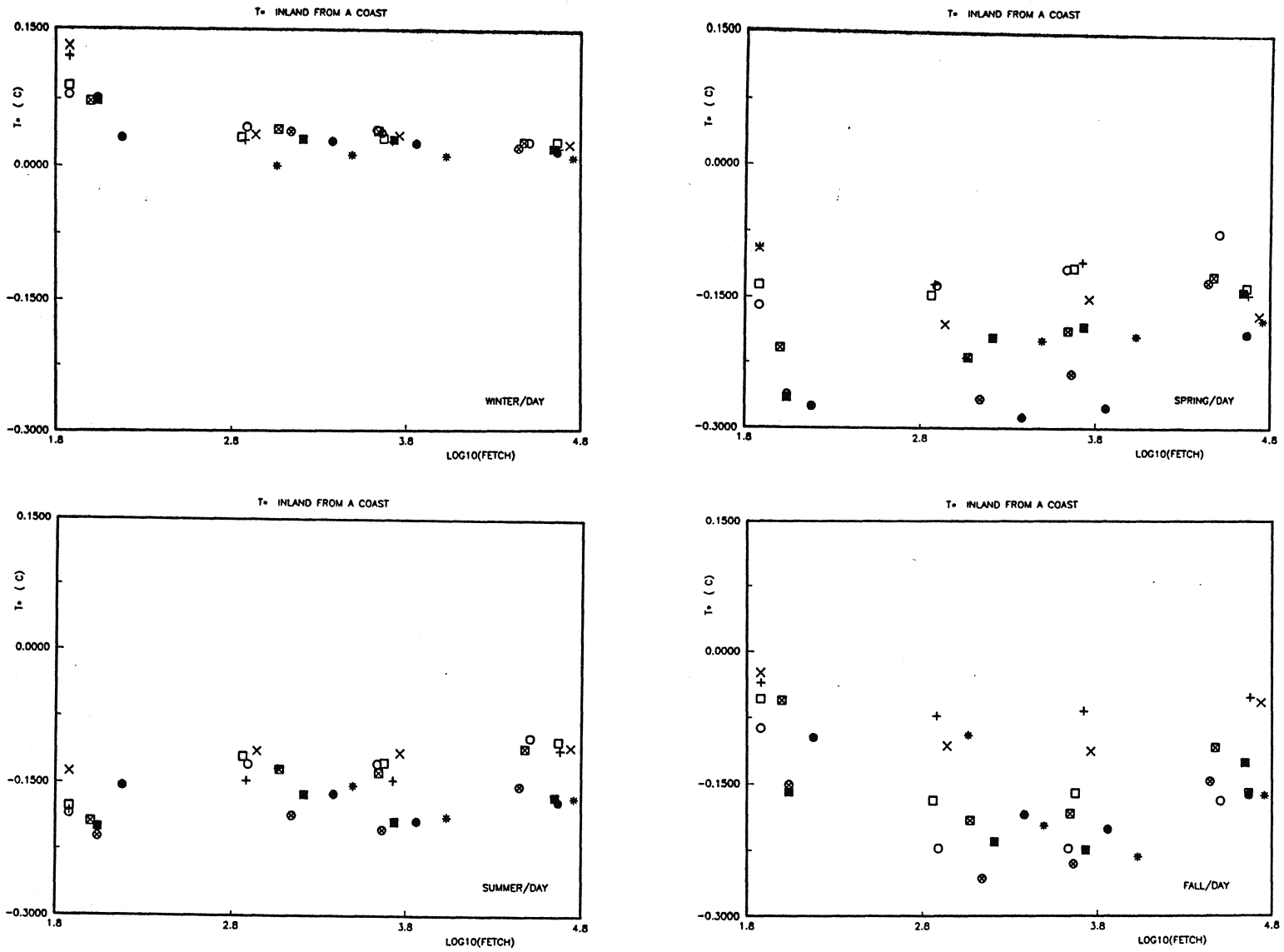

Figure 9c. The scale temperature, T_*, derived from the profiles of the masts and averaged for each mast, sector, season and day/night. Plotted versus fetch [m]. The symbols used refer to sectors, see table 4.

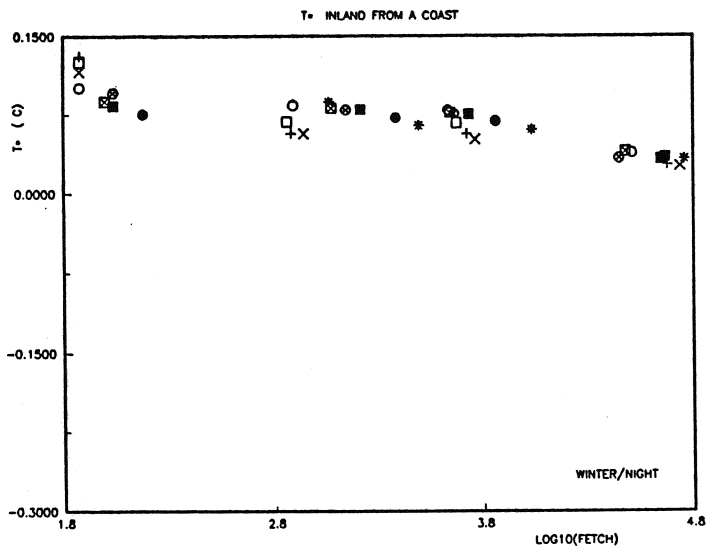

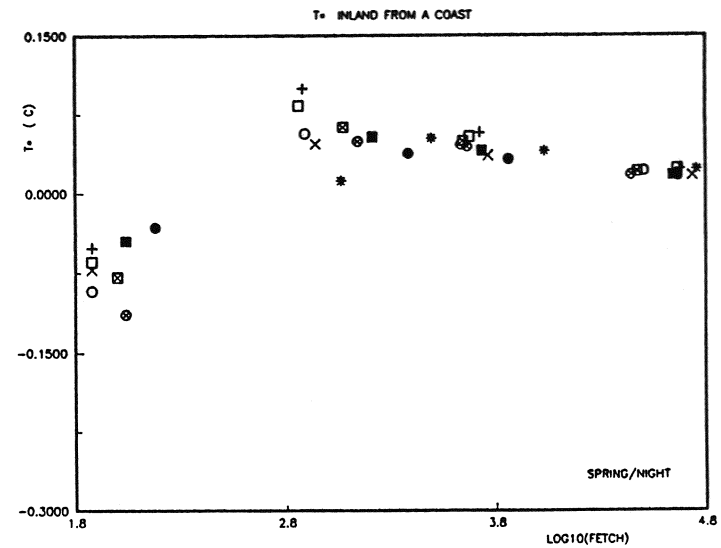

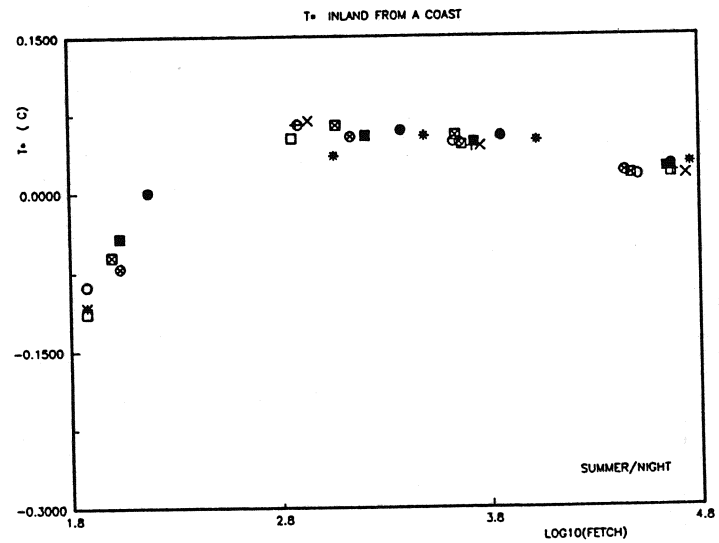

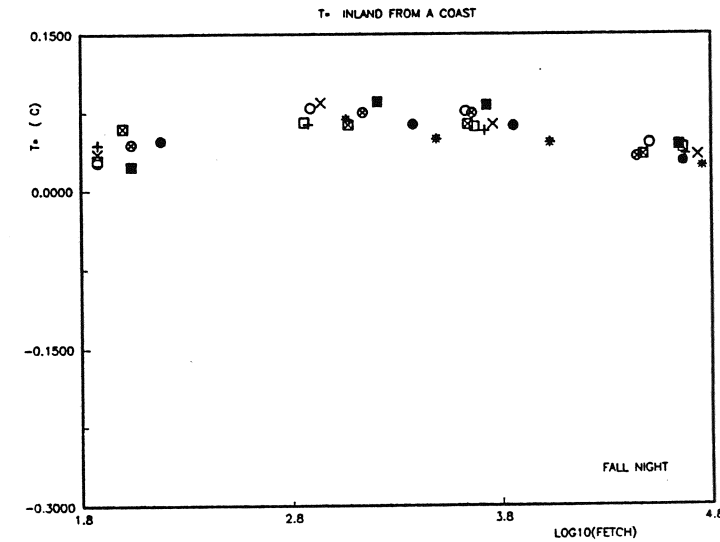

Figure 9d. As in figure 9c.

5.3 Friction velocity and turbulence temperature scale

Figures 9a, 9b, 9c and 9d show the parameters of friction velocity and turbulence temperature versus fetch, season and day or night. The friction velocity, u_*, and the scale temperature, T_*, are derived from the profiles measured, see Appendix A.

5.4 Heat Flux

During daytime we observe a different behaviour of the heat flux values for the different sectors. Using parameters pertaining to the SW directions, the heat fluxes calculated for masts 2, 3 and 4 are below the ones calculated using the NW wind parameter values, see figures 10a and 10b.

If we consider what is already discussed above for Fig. 6a, showing the seasonal global radiation, we know that it is higher with winds coming from the NW sectors, especially in the spring and fall. This point is confirmed also by the figures showing the nighttime heat flux where the spread of the data points disappears.

The absolute values of heat flux decrease going inland, especially at night. We will discuss this later together with the vertical and horizontal variation of the temperature.

The presence of an upwind water surface can be noted from the smaller variation of the heat flux calculated at mast 1 between day and night relative to the variation of the inland masts. Larsen and Gryning (1985) found that the influence of the sea extends up to 20 km inland, this could explain the different values for mast 4 in respect to masts 2 and 3.

5.5 Temperature

Vertical difference of Temperature

Figures 11a and 11b show the spatial variation of the vertical temperature. As seen from the figures, the absolute value of the vertical temperature gradient decreases when going inland.

Horizontal variation of temperature

Figures 12a and 12b show the horizontal variation of temperature for all four seasons and day/night. Temperature difference versus fetch is plotted: $\Delta T = T_1 - T_i$; $i = 2, 3, 4$ at 2 m height. Negative values for ΔT mean that the land surface is warmer and positive values that it is colder than the water surface.

In agreement with the results in Gryning and Batchvarova (1990) we found that by day the temperature increases going inland. In spring the increase is less than in fall, especially as concerns masts 2 and 3. We think that the heat capacity difference between sea and land plays an important role here. At night the temperature decreases inland, and in spring we see a faster decrease than in fall. Winter shows the same behaviour both during day and night. For the southern sectors the temperature increases inland while for the northern ones it decreases.

Heat flux, vertical and horizontal ΔT

The growth of a Temperature Internal Boundary Layer (TIBL) can be approached according to two different assumptions, e.g. Berkowicz (1988).

Some models relate the heat flux to differences between land and water temperature. Land temperature is constant with the distance from the water and the air temperature starts warming up and tends to reach the level of the land temperature further inland (figure 13a). In this way the heat flux decreases inland.

Other models relate the temperature difference between air and land to the solar radiation and the related turbulent heat flux, figure 13b. Solar radiation heats the land, and so the heat flux is constant and the vertical temperature difference is kept constant.

Unfortunately, we have no data on land and sea temperature. However, we do have quite extensive information on the behaviour of the different parameters inland as illustrated above.

It is seen from figure 13 that the inland variation of the heat flux is the most distinct difference between the step change in heat flux and that of surface temperature models.

In figure 14 we have therefore normalized the heat-flux plots of figure 10 by the average heat flux at mast 4. The figure indicates very strongly that the nighttime data seem definitely best described by the step change in the surface temperature model, while by day the data are somewhat closer to the step change in the heat flux model, at least in summer, fall and spring.

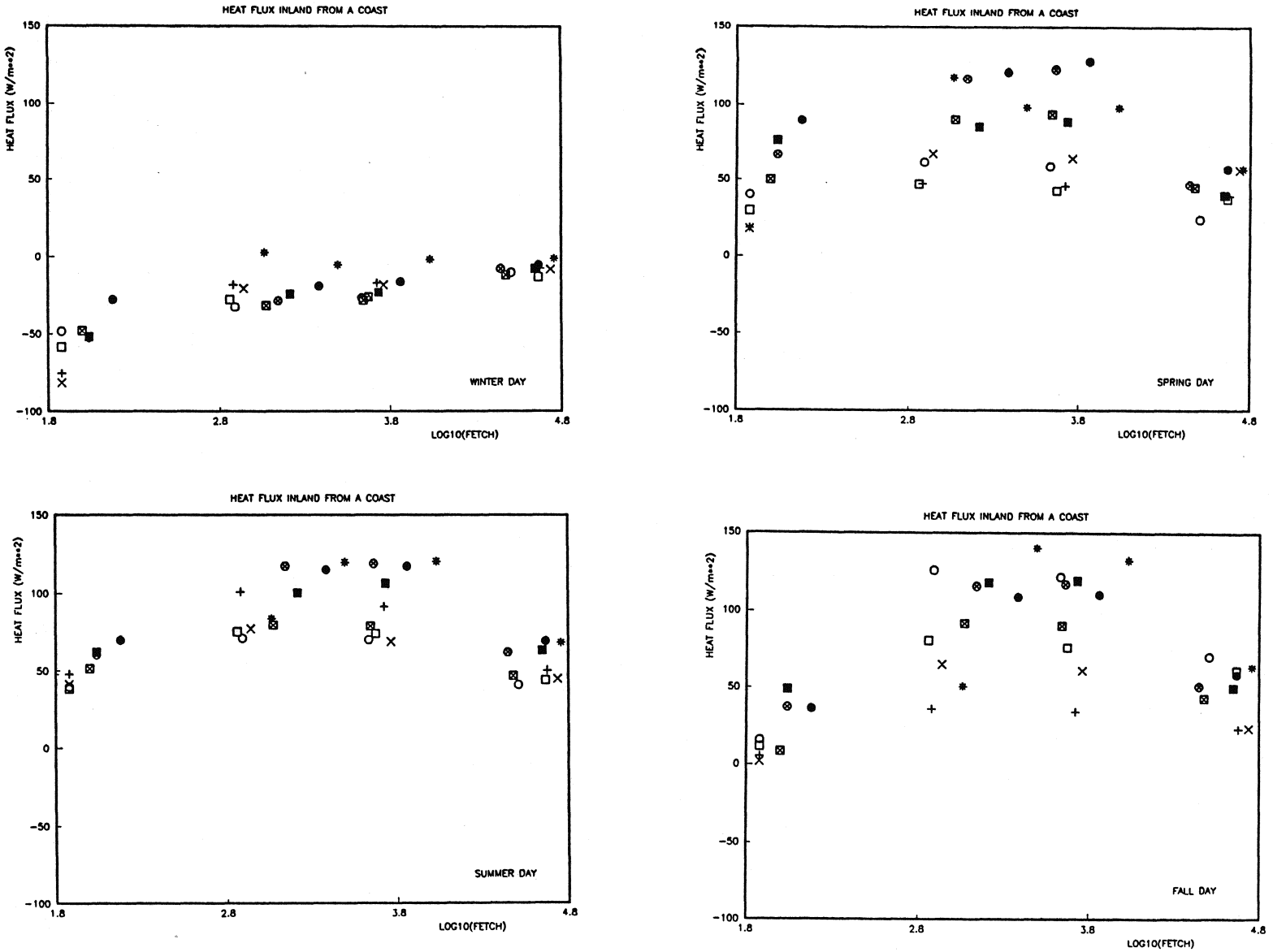

Figure 10a. Heat flux derived from velocity and temperature profiles averaged for each mast, sector, season and night/day, plotted versus logarithmic fetch (m). The symbols used are described in table 4.

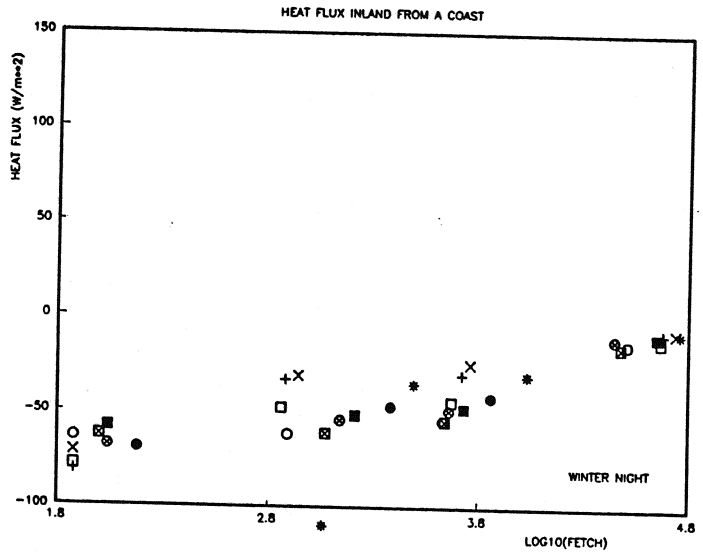

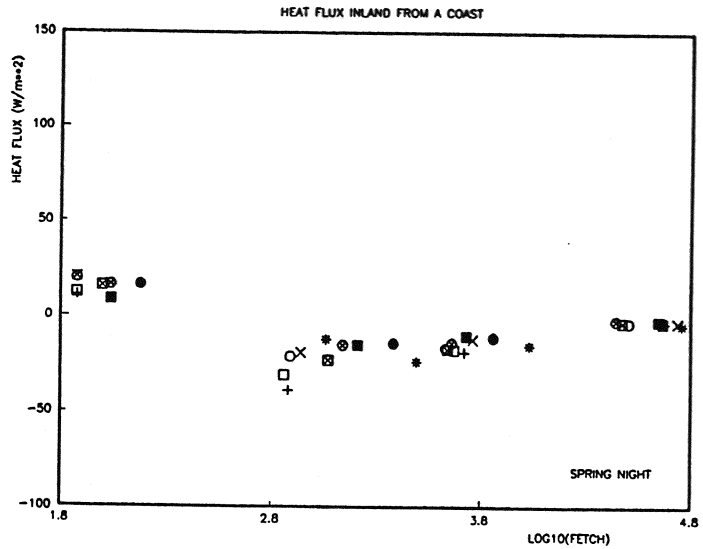

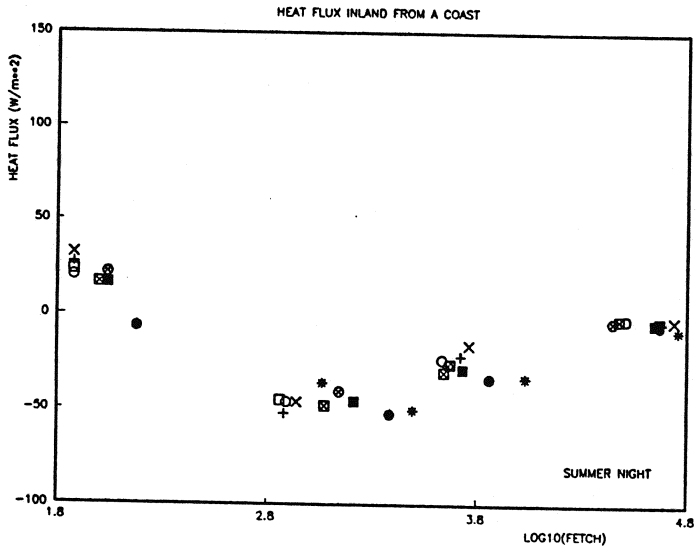

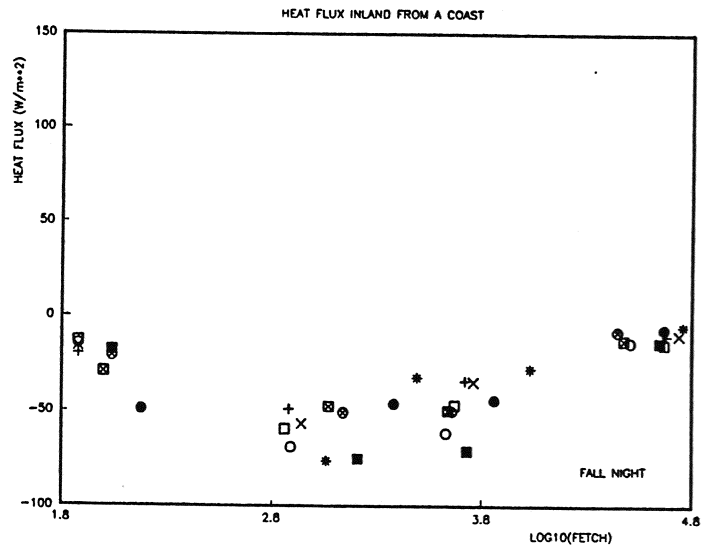

Figure 10b. As for figure 10a.

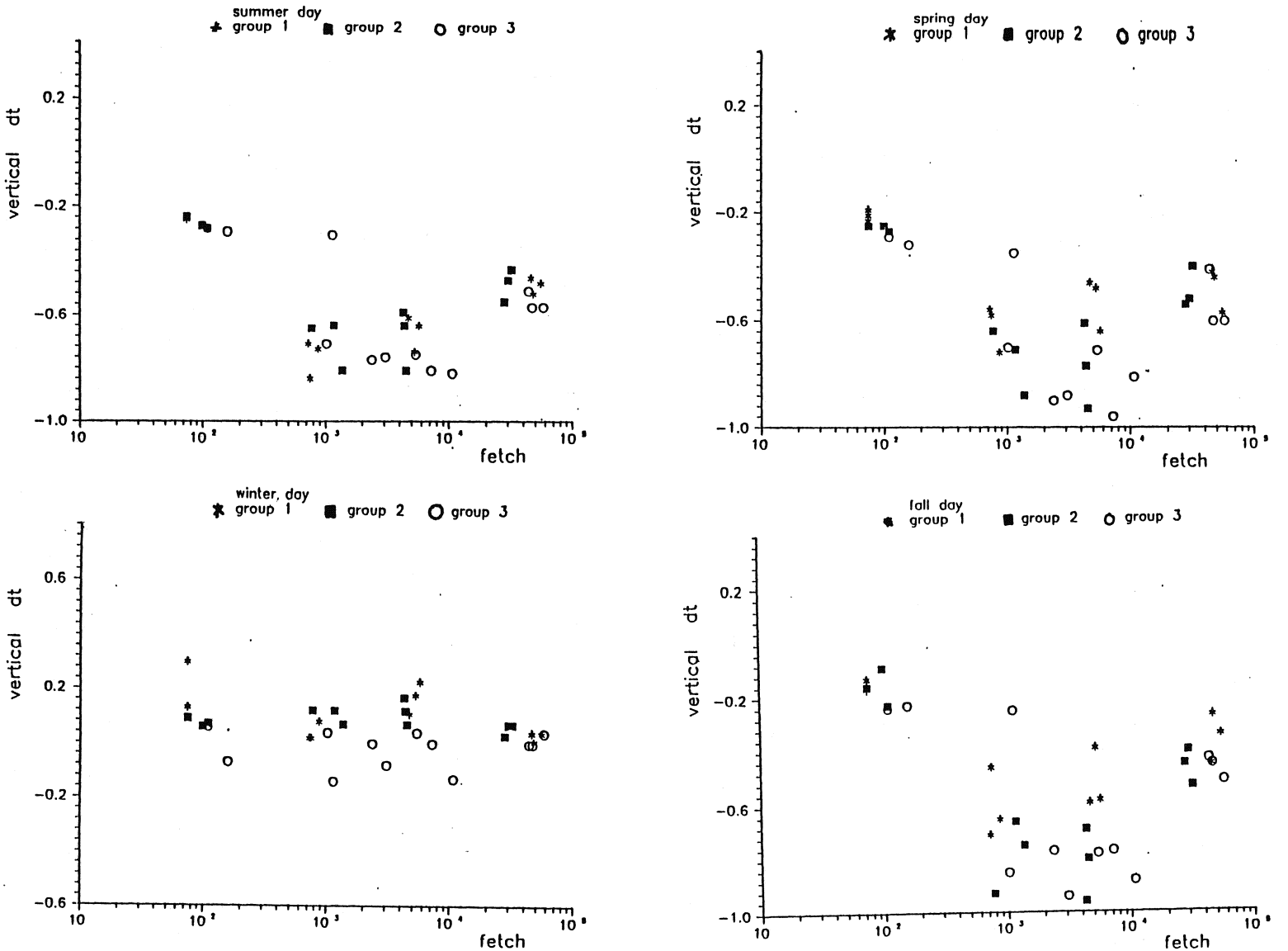

Figure 11a. Vertical temperature difference estimated and averaged for each mast, sector, season and day/night plotted versus fetch [m]. The data are arranged in three by three sectors, using only three symbols as described in table 4.

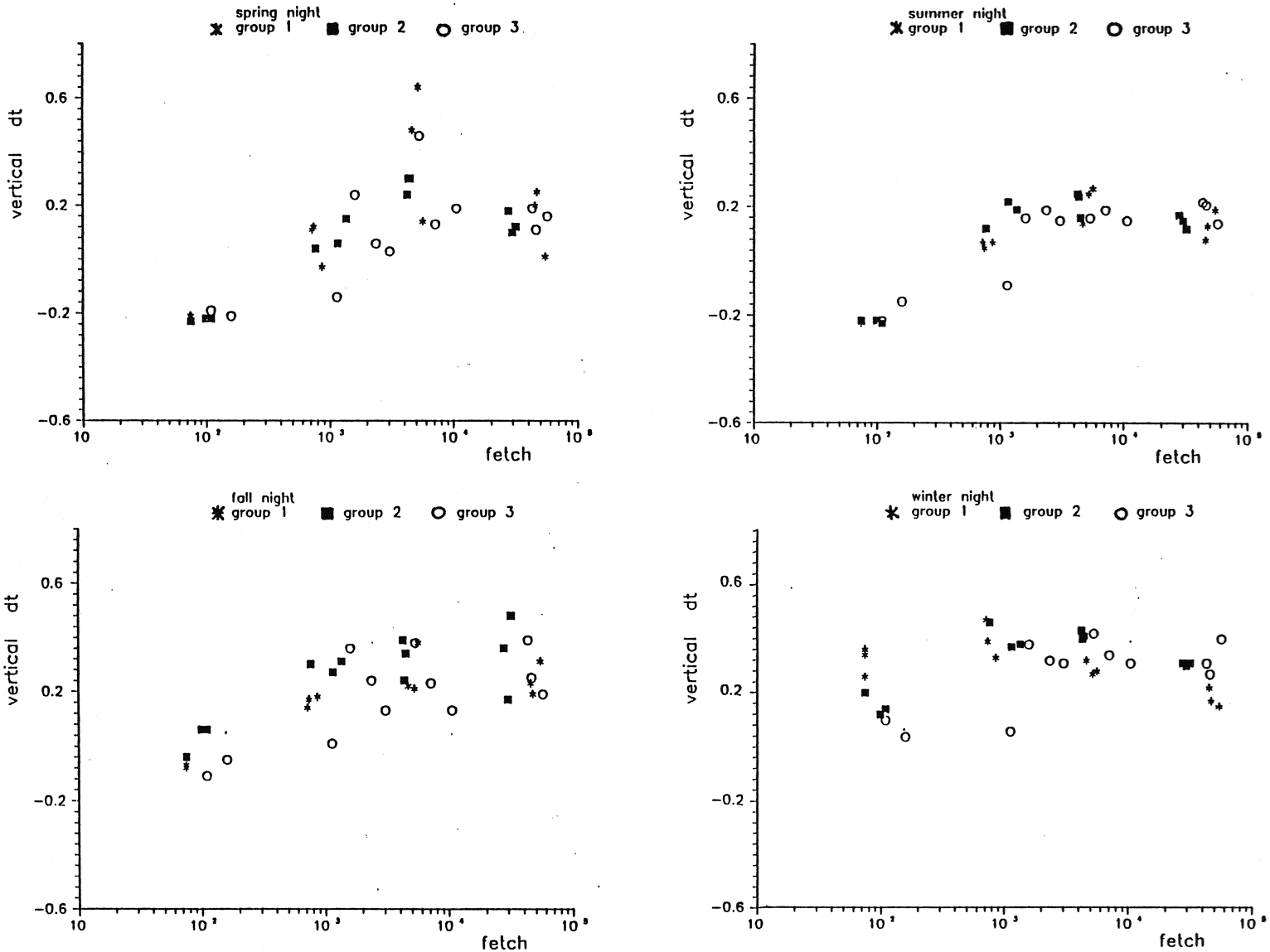

Figure 11b. As for figure 11a.

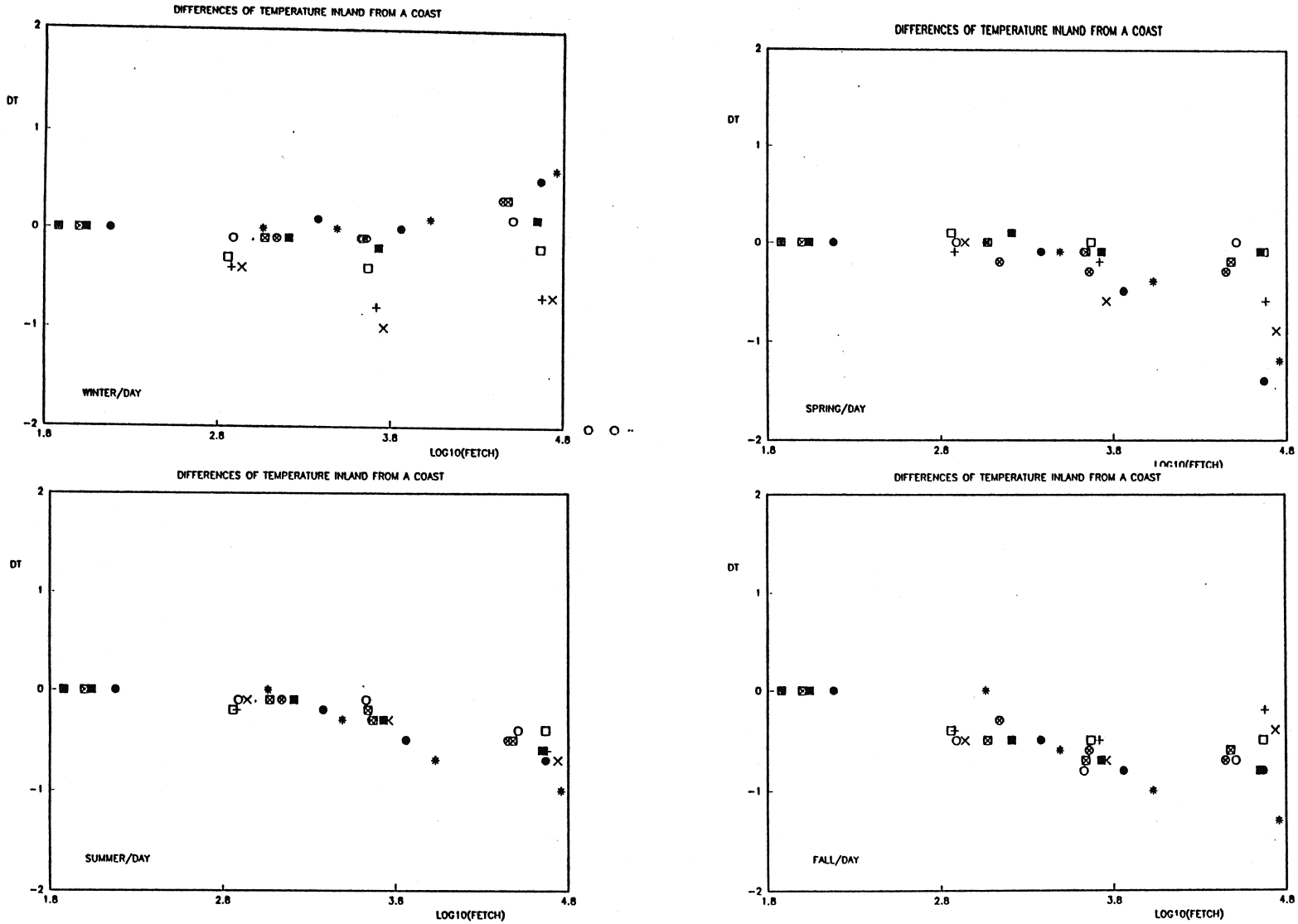

Figure 12a. Horizontal variation of the temperature 2 m above terrain, depicted as $\Delta T = T_1 - T_i$. Note that T_1 is the over-water temperature extrapolated as discussed in connection with table 2. The data are averaged for mast, sector, season, day/night and presented versus logarithmic fetch [m]. The symbols ar explained in table 4.

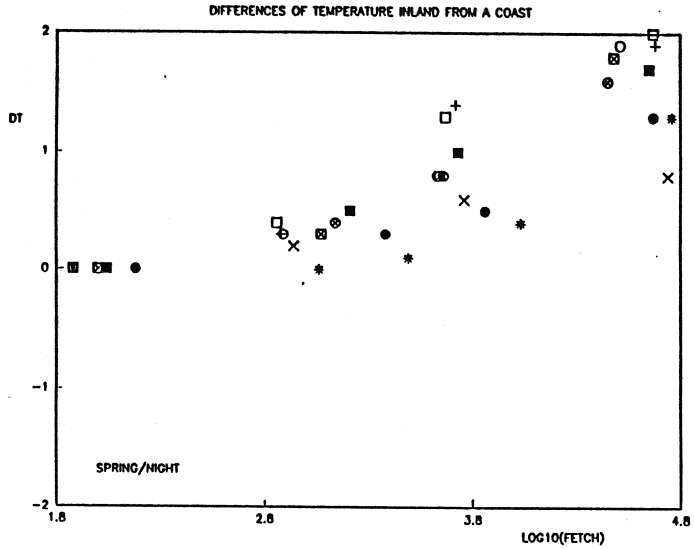

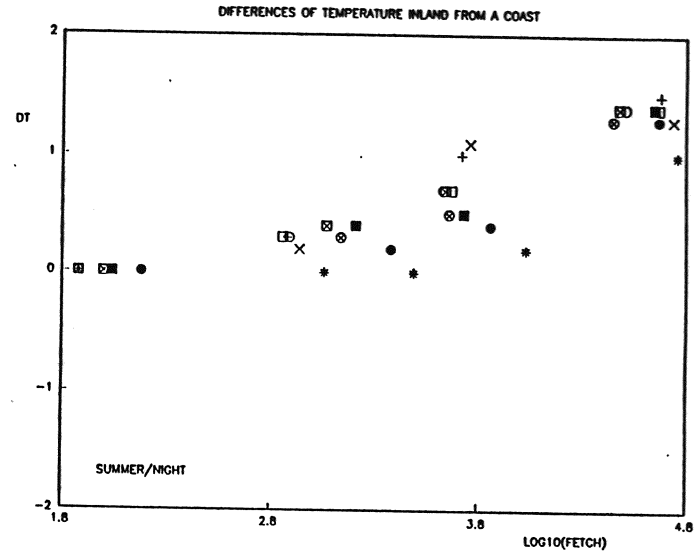

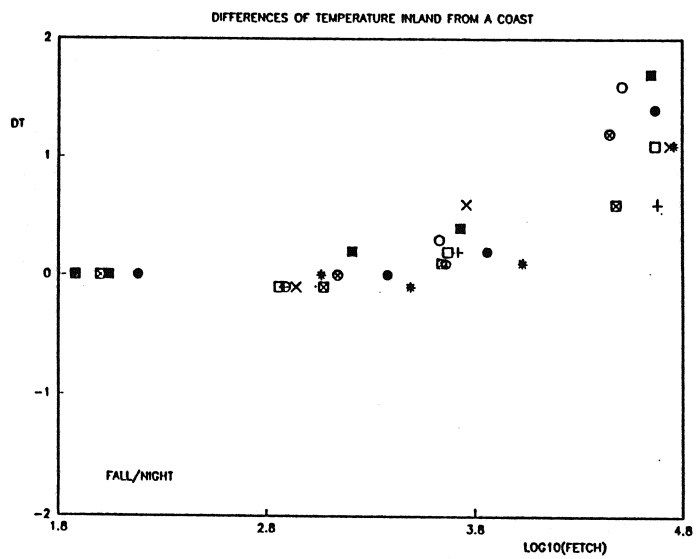

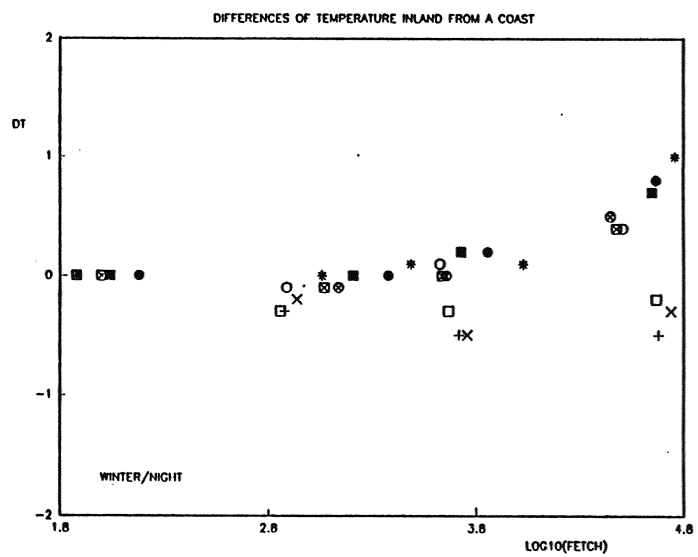

Figure 12b. As for figure 12a.

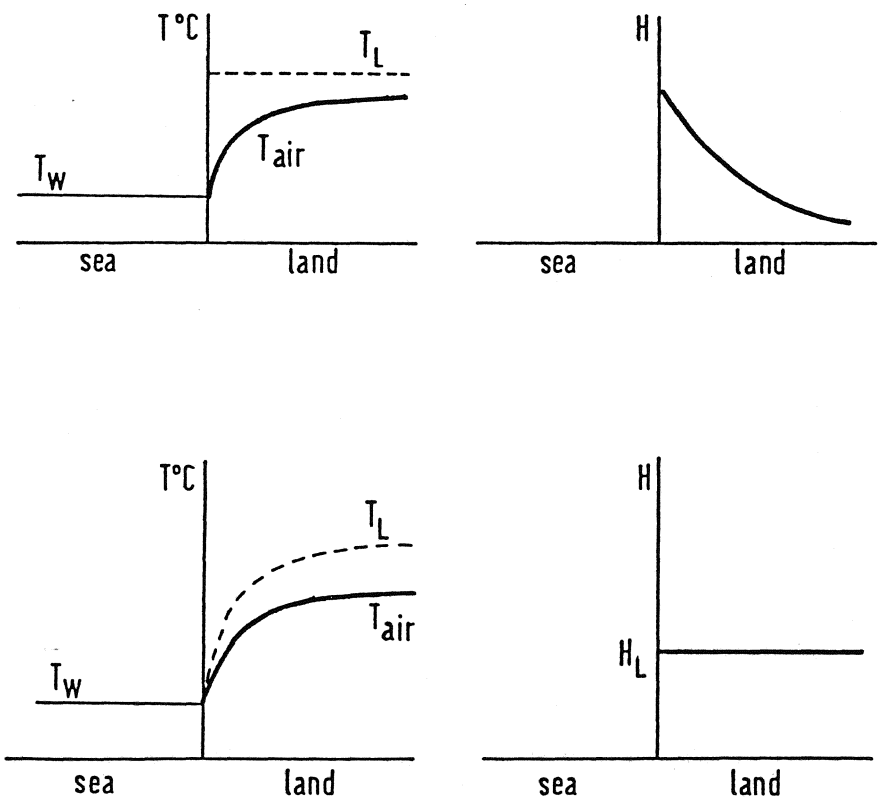

Figure 13. Two different descriptions of the development of a thermal internal boundary layer (Berkowicz, 1988). In figure 13a, the step change in surface temperature is considered, while figure 13b considers a step change in surface heat flux.

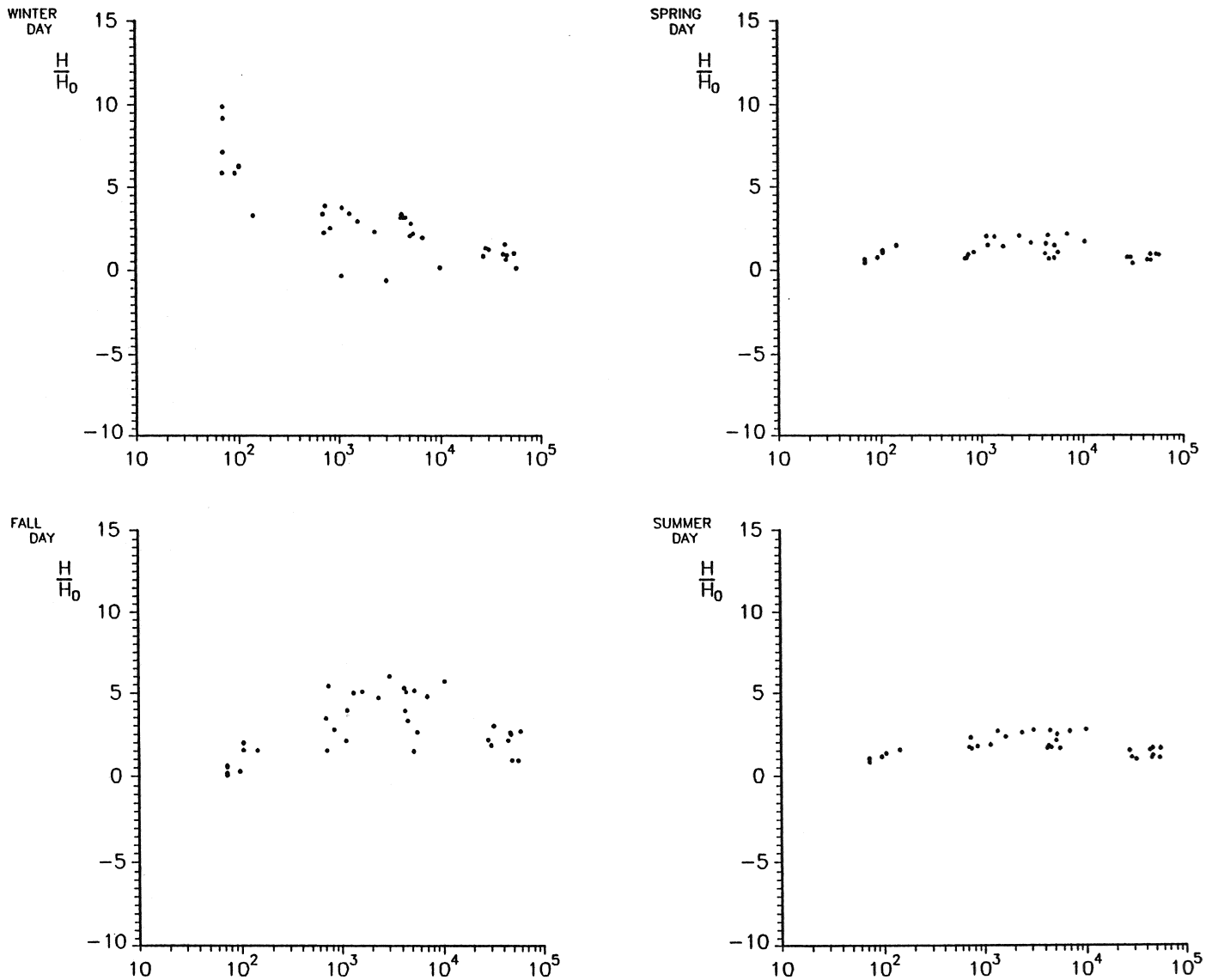

Figure 14a. Heat flux, H, at the different masts, normalized by the heat flux at mast 4, H_0, and plotted versus fetch.

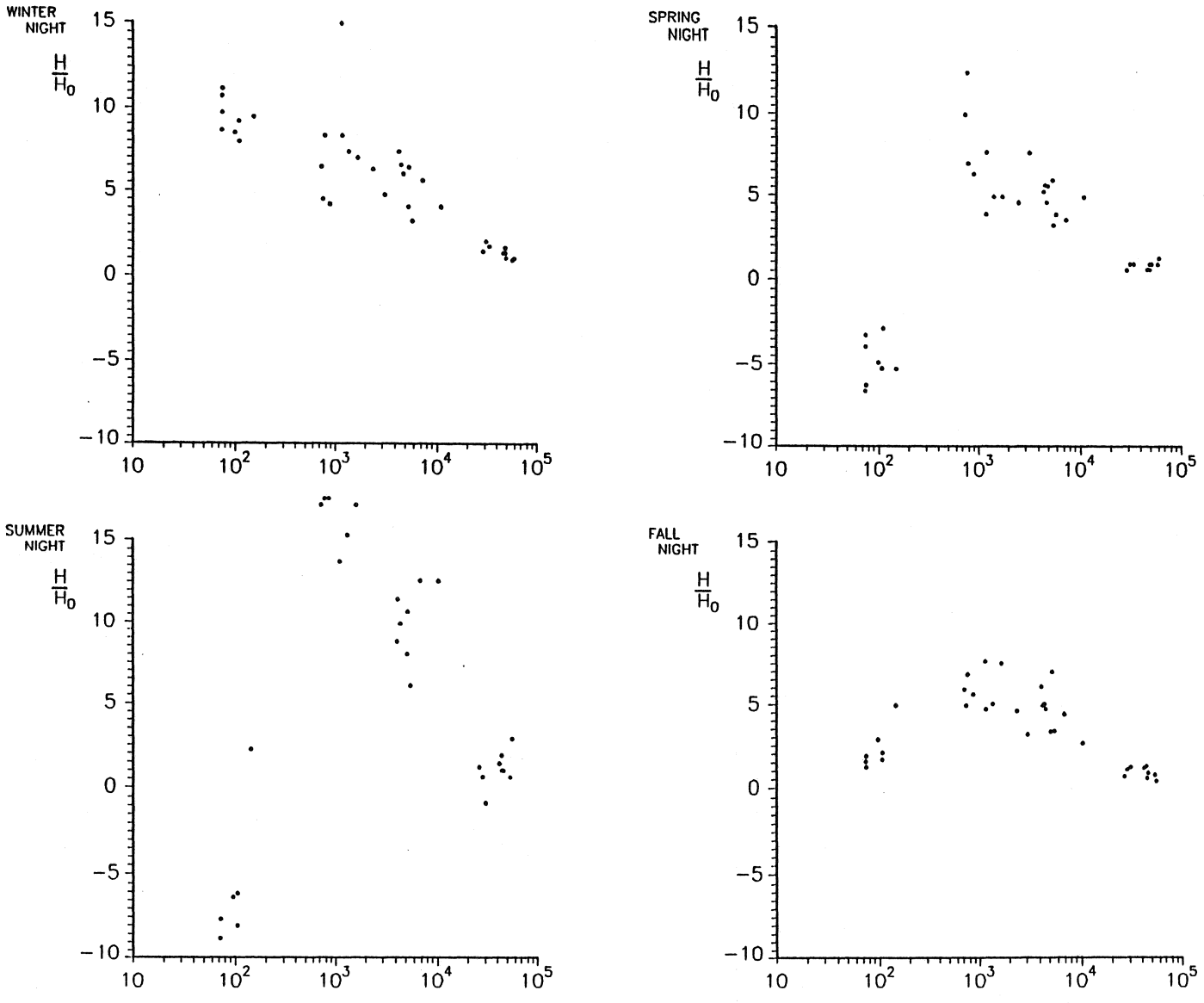

Figure 14b. As for figure 14a.

Acknowledgements

The authors would like to acknowledge Dr. Marisa Moriconi, Istituto di Fisica dell'Atmosfera del C.N.R., Rome for helpful discussions and Birthe Skrumsager for typing the manuscript in an orderly and well organized form.

References

Bergström, H., P. Johansson and A. Smedman (1988). A study of wind speed modification and internal boundary layer heights in a coastal region. *Boundary-Layer Meteorol.*, **42**, 313–335.

Berkowicz, R. (1988). Modelling the internal boundary layer at a coastal site. Appendix B to the report: Estimation of air pollution dispersion in an inhomogeneous terrain with special emphasis on coastal areas. (Eds. Berkowicz (main report in Danish) et al.), Air Pollution Laboratory, Risø National Laboratory.

Doran, J.C. and S.E. Gryning (1987). Wind and temperature structure over a land-water-land area. *J. Clim. Appl. Meteorol.*, **26**, 973–979.

Gryning, S.E. and E. Batchvarova (1990). Analytical model for the growth of the coastal internal boundary layer during onshore flow. *Quart. J. Roy. Meteorol.*, **116**, 187–203.

Larsen, S.E. and S.E. Gryning (1986). Dispersion climatology in a coastal zone. *Atmos. Environ.*, **20**, 1325–1332.

Larsen, S.E. and N.O. Jensen (1983). Summary and interpretation of some Danish climate statistics. Risø–R–399.

Larsen, S.E. and B. Nielsen (1991). Distribution of thermal stability classes over water and land in the Great Belt region (in preparation).

Mahrt, L. and S.E. Larsen (1982). Small scale drainage front. *Tellus*, **34**, 579–587.

Ogawa, Y and T. Ohara (1985). The turbulent structure of the internal boundary layer near the shore. Part 1: Case Study. *Boundary-Layer Meteorol.*, **31**, 369–384.

Sempreviva, A.M., S.E. Larsen, N.G. Mortensen and I. Troen (1988). Roughness change effects for small and large fetches. Risø–M–2749, 49 pp.

Sempreviva, A.M., S.E. Larsen, N.G. Mortensen and I. Troen (1990). Response of neutral boundary layers to changes of roughness. *Boundary-Layer Meteorol.*, **50**, 205–225.

Van Wijk, A.J.M., A.C.M. Beljaars, A.A.M. Holtslag and W.C. Turkenburg (1990). Diabatic wind speed profiles in coastal regions: comparison of an internal boundary layer (IBL) model with observations. *Boundary-Layer Meteorol.*, **51**, 49–75.

Appendix A: Description of profile relations

The Richardson number is defined by

$$Ri = \frac{g}{T}\frac{\frac{dT}{dz} + \Gamma}{\left(\frac{du}{dz}\right)^2} \tag{A.1}$$

where

Γ	=	adiabatic lapse rate
T	=	temperature
u	=	wind speed
z	=	vertical coordinate, and
g	=	acceleration due to gravity.

Ri has been calculated at the logarithmic mean height

$$z_{\mathrm{LMH}} = \frac{z_1 z_2}{z_1 + z_2} \tag{A.2}$$

and then referred to the 10-m level

$$R_z = \frac{R_{\mathrm{LMH}}}{z_{\mathrm{LMH}}} \cdot 10 \tag{A.3}$$

The heat flux, H, has been derived from the profiles as

$$H = -\rho c_p T_* u_* \tag{A.4}$$

where

ρ	is air density
c_p	is its specific heat at constant pressure while T_* and u_* are the turbu-
ρc_p	is heat capacity

lence temperature scale and friction velocity, respectively. To calculate T_* and u_* we used the following formulation

$$u_* = \Delta u \kappa left[\ln\frac{z_2}{z_1} - \Psi_M\left(\frac{z_2}{L}\right) + \Psi_M\left(\frac{z_1}{L}\right)^{-1} \tag{A.5}$$

where Ψ_M is the similarity function for the mechanics momentum

$$\Psi_M = 2\ln\left(\frac{1+x}{2}\right) + \ln\left(\frac{1+x^2}{2}\right) - 2\arctan(x) + \frac{\pi}{2} \tag{A.6}$$

where

$$x = \left(1 - 16\left(\frac{z}{L}\right)\right)^{1/4}$$

for the instable case, Dyer and Hicks, and

$$\Psi_M = -5\frac{z}{L}$$

for stable cases. For L we used the following formulation

$$T_* = \Delta\Theta \cdot \kappa \cdot \left(\ln\frac{z_2}{z_1} - \Psi_H\left(\frac{z_2}{L}\right) + \Psi_H\left(\frac{z_1}{L}\right)\right) \tag{A.7}$$

where $\Delta\Theta$ is the potential temperature difference between level z_2 and z_1.

$$\Delta\Theta = \Delta T + 0.0098\Delta z \tag{A.8}$$

where

ΔT is the temperature difference measured between z_1 and z_2 and
$\Psi_H(z/L)$ is the similarity function for the temperature profile

$$\Psi_H = -5\frac{z}{L} \qquad Ri > 0$$

$$\Psi_H = 2\ln\left(\frac{1+\Upsilon(z/L)}{2}\right) \qquad Ri < 0$$

where

$$\Upsilon(z/L) = \left(1 - 16\frac{z}{L}\right)^{-1/2} \qquad \text{Dyer and Hicks.}$$

For stable cases the Monin-Obukhov length, L, has been calculated using (Larsen and Nielsen, 1991)

$$\frac{z}{L} = \varphi_m \, Ri \, \frac{K_H}{K_M} \tag{A.9}$$

where

$$\frac{K_H}{K_M} = \frac{(1+Ri)}{(1+Ri+t\,Ri^2)}$$

$$\varphi_m = \frac{1}{1-5\left(\frac{K_H}{K_M}\right)Ri} \qquad 0 < Ri < 0.2$$

$$1 + 24 \cdot 4\,Ri \qquad Ri > 0.2$$

(A.10)

This formulation has been used when calculating L, using the Richardson number so as to avoid L being infinitive which would result in negative values for $Ri > 0.2$.

Bibliographic Data Sheet **Risø–M–2924(EN)**

Title and author(s)

Experimental Study of Flow Modification Inland from a Coast for Nonneutral Conditions

Anna M. Sempreviva, S.E. Larsen and N.G. Mortensen

ISBN	ISSN
87–550–1719–3	0418–6435

Dept. or group	Date
Meteorology and Wind Energy	January 1992

Groups own reg. number(s)	Project/contract No.

Pages	Tables	Illustrations	References
41	4	14	12

Abstract (Max. 2000 char.)

During a two-year period measurements were obtained along four meteorological masts placed from the coastline to 30 km inland at the North Sea coast of Jutland in Denmark (the JYLEX experiment).
The data were organized to show the behaviour of the most important parameters of the turbulent structure when a flow passes from over-sea to over-land conditions. The results are stratified according to season, day and night, and wind direction.

Descriptors INIS/EDB

BOUNDARY LAYERS; COASTAL REGIONS; HEAT FLUX; METEOROLOGY; NUMERICAL DATA; SEASONAL VARIATIONS; TURBULENT FLOW; VELOCITY; WIND

Available on request from:
Risø Library, Risø National Laboratory (Risø Bibliotek, Forskningscenter Risø)
P.O. Box 49, DK–4000 Roskilde, Denmark
Phone (+45) 42 37 12 12, ext. 2268/2269 · Telex 43 116 · Telefax (+45) 46 75 56 27